The Journal of Chemical Physics

RESEARCH ARTICLE | SEPTEMBER 30 2019

Adaptive strong-field control of vibrational population in NO^{2+}

O. Voznyuk; Bethany Jochim ; M. Zohrabi ; Adam Broin; R. Averin; K. D. Carnes ; I. Ben-Itzhak ; E. Wells

Check for updates

J. Chem. Phys. 151, 124310 (2019)
https://doi.org/10.1063/1.5115504
CHORUS

View Online
Export Citation
CrossMark

Articles You May Be Interested In

High-time resolution measurements of solar wind heavy ions with SOHO/CELIAS/CTOF

AIP Conference Proceedings (March 2016)

Observations of the He^+ pickup ion torus velocity distribution function with SOHO/CELIAS/CTOF

AIP Conference Proceedings (March 2016)

SOHO CTOF Observations of Interstellar He^+ Pickup Ion Enhancements in Solar Wind Compression Regions

AIP Conference Proceedings (September 2003)

25 September 2023 21:20:00

500 kHz or 8.5 GHz?
And all the ranges in between.
Lock-in Amplifiers for your periodic signal measurements

Find out more
Zurich Instruments

AIP Publishing

The Journal of Chemical Physics ARTICLE scitation.org/journal/jcp

Adaptive strong-field control of vibrational population in NO^{2+}

Cite as: J. Chem. Phys. 151, 124310 (2019); doi: 10.1063/1.5115504
Submitted: 18 June 2019 • Accepted: 10 September 2019 •
Published Online: 30 September 2019

View Online Export Citation CrossMark

O. Voznyuk,[1,a] Bethany Jochim,[1,2,a] M. Zohrabi,[2] Adam Broin,[1] R. Averin,[1] K. D. Carnes,[2] I. Ben-Itzhak,[2] and E. Wells[1,b]

AFFILIATIONS

[1] Department of Physics, Augustana University, Sioux Falls, South Dakota 57197, USA
[2] J.R. Macdonald Laboratory, Department of Physics, Kansas State University, Manhattan, Kansas 66506, USA

[a] **Contributions:** O. Voznyuk and B. Jochim contributed equally to this work.
[b] **Electronic mail:** eric.wells@augie.edu

ABSTRACT

An adaptive closed-loop system employing coincidence time-of-flight feedback is used to determine the optimal pulse shapes for manipulating the branching ratio of NO dications following double ionization by an intense laser pulse. Selection between the long-lived NO^{2+} and the dissociative $N^+ + O^+$ final states requires control of the vibrational population distribution in the transient NO^{2+}. The ability to both suppress and enhance NO^{2+} relative to $N^+ + O^+$ is observed, with the effectiveness of shaped pulses surpassing near Fourier transform-limited pulses by about an order of magnitude in each direction, depending on the pulse energy. The control is subsequently investigated using velocity map imaging, identifying plausible dissociation pathways leading to $N^+ + O^+$. Combining the information about the $N^+ + O^+$ dissociation with a well-defined control objective supports the conclusion that the primary control mechanism involves selectively populating long-lived NO^{2+} vibrational states.

https://doi.org/10.1063/1.5115504

25 September 2023 21:20:00

I. INTRODUCTION

In adaptive femtosecond control experiments,[1–3] measurement-based feedback is used in conjunction with a learning algorithm to tailor an ultrafast laser pulse to optimize a particular process. While adaptive femtosecond control has been widely applied,[4–19] controlling the photofragmentation and rearrangement of molecules in the gas phase has been an area that has received particular attention.[3,20–33] Nearly all of these experiments describe an ability to influence the fragmentation patterns of the target molecules, but only a smaller subset report progress toward understanding the mechanisms underlying the control.[34–47] Given the complexity of the intense laser-molecule interaction and the nearly infinite variety of laser pulses that can be produced by modern pulse shaping devices,[48–50] it is not surprising that unraveling the physical process behind the control is often difficult.

In many of these molecular fragmentation experiments, the feedback signal is derived from fragment ion yields acquired via time-of-flight (TOF) mass spectrometry. The advantages of this method are clear; the data acquisition is relatively straightforward, and when a current mode is employed (as opposed to counting individual ions), the yields may be obtained quickly, which is generally a requirement for effective feedback in adaptive control experiments. These single fragment yields, however, are uncorrelated, and so it becomes difficult to separate various final products. A somewhat simplistic example of this problem is illustrated by a hypothetical molecule AB, for which the $A^+ + B^+$ channel cannot generally be separated from the $A^+ + B$ channel since both contribute to the A^+ yield.

In addition, a large intensity range is present in the focal volume. The range of contributing intensities can be reduced by operating near the appearance intensity of a process, but this is often incompatible with the experimental desire for timely feedback in closed-loop control. Subsequent interpretation of the results can then become convoluted due to the ambiguities in the intensity and photofragment channel. More specific control objectives can focus

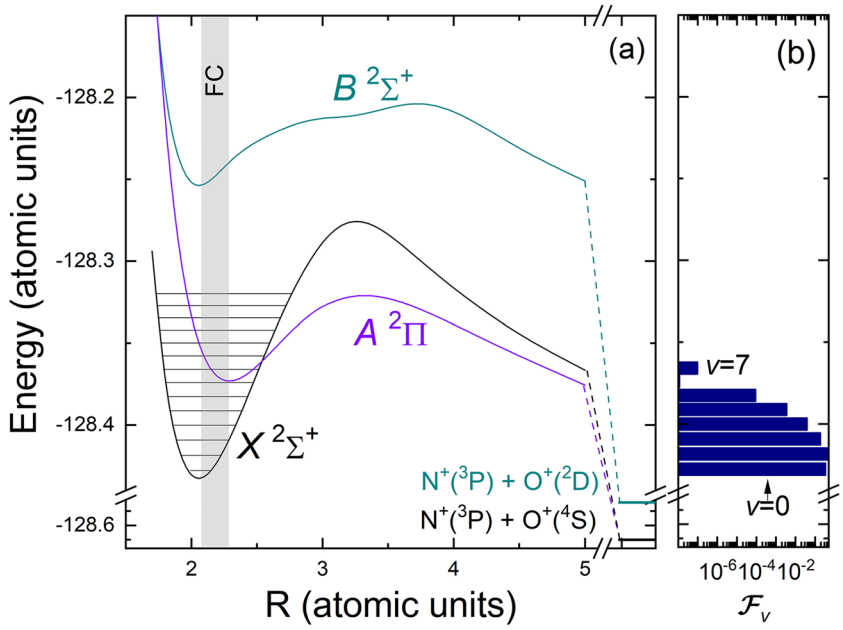

FIG. 1. (a) The lowest lying doublet potential energy curves for NO^{2+}, adapted from Ref. 53. The energies at the separate atom limit are −128.65 a.u. for the $X\ ^2\Sigma^+$ and $A\ ^2\Pi$ states and −128.52 a.u. for the $B\ ^2\Sigma^+$ state. The shaded box marks the region of vertical Franck-Condon (FC) transitions from neutral NO. (b) Franck-Condon populations for the $X\ ^2\Sigma^+$ state of NO^{2+} assuming field-free NO → NO^{2+} vertical ionization.

the search process on a more limited set of pathways and intensity range and therefore inform efforts to understand the resulting solution produced by the learning algorithm.

We have developed a coincidence time-of-flight feedback (CTOF) technique[51] to provide more specific feedback for closed loop control. In our initial experiment with this CTOF feedback, we enhanced or suppressed the ratio of CO^{2+} to $C^+ + O^+$ following strong-field double ionization of CO molecules. This was particularly interesting in CO^{2+}, since only the $v = 0$ and $v = 1$ states of the $^3\Pi$ ground state and the $v = 0$ state of the lowest $^1\Sigma^+$ state live long enough to be detected as CO^{2+} in our experimental setup, while all the higher vibrational states rapidly decay to $C^+ + O^+$. Thus, the ability to unambiguously select between CO^{2+} and $C^+ + O^+$ represented control of vibrational population.

As shown in Fig. 1, NO^{2+} is somewhat similar to CO^{2+} in that higher vibrational levels ($v > 12$) of the $X\ ^2\Sigma^+$ ground electronic state dissociate within 18 ns due to spin-orbit coupling with the $A\ ^2\Pi$ state. The $v \geq 8$ vibrational states of the $A\ ^2\Pi$ excited electronic state decay by tunneling with a lifetime less than or equal to ~45 ns.[52] In addition, these two states are easily coupled by one-photon transitions, leading to dissociation, while the $B\ ^2\Sigma^+$ state is well separated from the $X\ ^2\Sigma^+$ and $A\ ^2\Pi$ states. Experimentally, the $N^+ + O^+$ and NO^{2+} channels offer similar feedback as the initial CO experiment,[51] but the increased complexity of the relevant potential energy curves provides an additional interpretation challenge.

With this increased complexity in mind, we have employed velocity map imaging[54–58] (VMI) to examine the differences in the three-dimensional momentum images produced by unshaped and optimized laser pulses. In diatomic molecules, the angle-resolved kinetic energy release (E_k) data can be used in conjunction with a Floquet approach[59–61] to understand which dissociation pathways are enhanced by the optimized pulses. Our first efforts using this combination of VMI measurements and Floquet analysis resulted in an improved understanding of control experiments with CO molecules.[62]

In this article, we discuss the results from adaptive femtosecond control experiments using CTOF feedback to control the vibrational population of the transient NO^{2+} molecular ion. We are able to either increase or decrease the $NO^{2+}/(N^+ + O^+)$ ratio by approximately an order of magnitude, primarily through suppression or enhancement of the NO^{2+} yield. The results are then analyzed with the aid of VMI measurements of the dissociating N^+ and O^+ photofragments, as well as kinetic energy release distributions evaluated from coincidence time-of-flight measurements.

II. EXPERIMENTAL METHOD

Our experimental setup consists of an ultrafast laser system equipped with an acousto-optic programmable dispersive filter (AOPDF)[49] pulse shaping device and a high resolution time-of-flight mass spectrometer, linked by a control computer running the genetic algorithm (GA) that uses the feedback signals to determine the optimal pulse shapes. This is illustrated in Fig. 2(a). The laser pulses are provided by a Ti:sapphire laser system with a center wavelength of 788 nm, a pulse energy of approximately 1 mJ, and a repetition rate of 2.0 kHz. The near-Fourier transform-limited (FTL) pulse duration is approximately 40 fs (FWHM in intensity) following passage through the AOPDF, multipass amplifier, and transport optics to the vacuum chamber. In these measurements, the AOPDF was only used to control the spectral phase, and therefore, the pulse energy remains constant as the pulse characteristics are changed (note that the pulse intensity changes as pulse duration is modified). Laser pulse characteristics were measured using second harmonic generation frequency-resolved optical gating (SHG FROG).[50,63]

25 September 2023 21:20:00

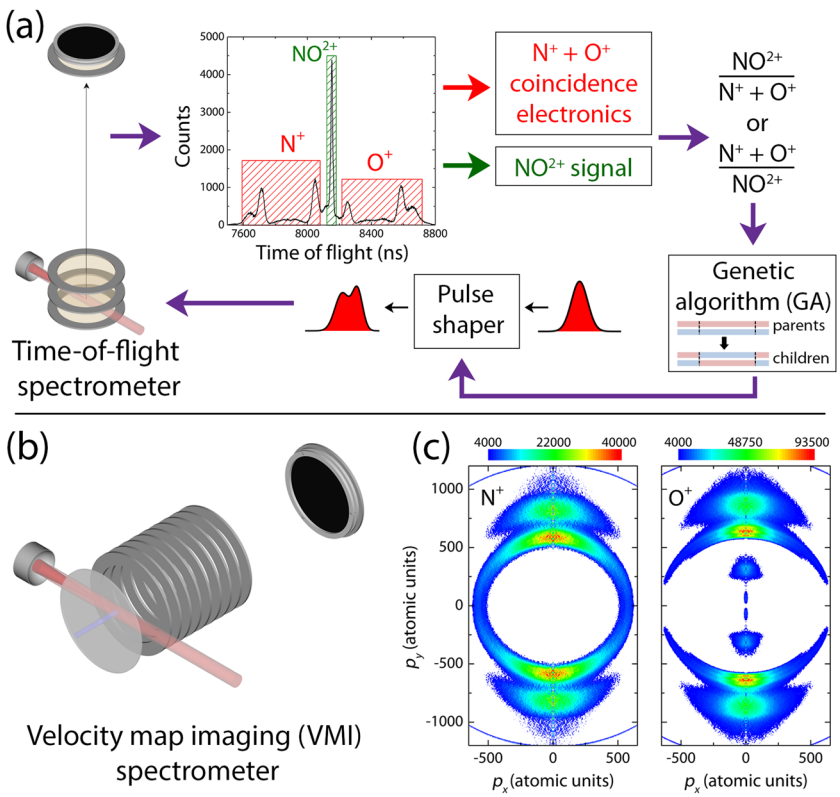

FIG. 2. (a) A schematic of the CTOF closed-loop control scheme. The NO^{2+} ions were measured along with coincident $N^+ + O^+$ events using a high-resolution TOF spectrometer.[51] The boxes on the TOF spectra conceptually represent the gates on the ions of interest. (b) Once the optimal pulses were identified, the interaction between the pulses and NO was probed with velocity map imaging in a different spectrometer.[58,62,64] The laser pulses were focused into the CTOF and VMI spectrometers by identical f = 75 mm spherical mirrors. By matching the incoming laser beam diameters, the focal conditions were similar in both measurements. (c) Momentum distributions of N^+ (left) and O^+ (right) photofragments obtained via velocity map imaging. The laser polarization direction is in the y-direction in both panels. The data presented are for measurements using FTL laser pulses at 0.04 mJ/pulse or approximately 5×10^{14} W/cm^2. While VMI provides angular information, it lacks the coincidence condition that identifies the $N^+ + O^+$ channel.

The laser beam was focused by an f = 75 mm spherical mirror to a point in the extraction region of a two-stage Wiley-McLaren[65] time-of-flight (TOF) spectrometer. In most of these experiments, the pulse energy was attenuated to between 0.02 and 0.06 mJ, although some data were recorded at higher pulse energy. This translates to a peak intensity of about $3–8 \times 10^{14}$ W/cm^2 for a FTL pulse and a beam waist of ~10 μm. The TOF spectrometer is located in an ultra-high vacuum chamber that had a base pressure of about 5×10^{-10} Torr. Typical target pressures for the experiment were in the low 10^{-8} Torr range and were adjusted using a precision leak valve to control the counting rate. The laser beam was linearly polarized with the polarization parallel to the TOF spectrometer axis. Ions were detected by a microchannel plate (MCP) detector.[66] Importantly, the spectrometer did not use a small aperture along the polarization (TOF) axis as is often the case in laser-initiated TOF measurements (for example, in one of our previous experiments[67]), therefore avoiding discrimination in the angular distribution of the resulting ions.

As described more fully in a previous publication,[51] the signals from the MCP are processed on-the-fly to determine the NO^{2+} and coincident $N^+ + O^+$ rates that are used to determine the fitness value for the control objective. A photodiode monitors the laser pulses and that timing signal is converted to a NIM-standard pulse via a constant fraction discriminator and delayed until shortly before the N^+ arrival time on the MCP. This delayed photodiode signal starts three time-to-amplitude converters (TAC). The MCP signals are amplified, processed by a constant fraction discriminator, and used as the stop signals on each of the TACs. Each TAC is used in single-channel analyzer mode, producing an output only in cases in which the ion signal falls within a specified time window appropriate for N^+, NO^{2+} and O^+ events. The O^+ TAC is gated by the condition that the N^+ TAC has produced an output signal, thus producing a signal for $N^+ + O^+$ coincidence events. The rates from the NO^{2+} and the gated O^+ TAC outputs are converted to an analog signal, averaged over some time constant (typically about 5–10 s), and sent to the control computer. These rates are used to evaluate the "fitness" of the GA control objective: $NO^{2+}/(N^+ + O^+)$ or $(N^+ + O^+)/NO^{2+}$.

Our GA implements tournament selection, two-point crossover, elitism, and a moderate 1% mutation rate per gene.[43,51,58] Typically, 40–50 individuals populate each generation, and the algorithm ran for 20–40 generations, depending on the convergence rate and the laser stability. A constant, approximately equal to 10% of the denominator channel of the control objective obtained with a FTL pulse, is used to prevent high fitness values when no denominator signal is present.

Once the closed-loop adaptive control measurement has optimized the pulse shape corresponding to a particular control objective, the result is examined using two other techniques. First, the TOF spectrum is recorded using a time-to-digital converter in full multihit mode, thus correlating all the "stop" signals associated with a single "start" signal from the photodiode that monitors the laser pulse. This allows more precise measurements of the true coincidence rate since random coincidences (N^+ and O^+ pairs that do not arise from the same molecule) and lost fragments (ion-pairs in which

25 September 2023 21:20:00

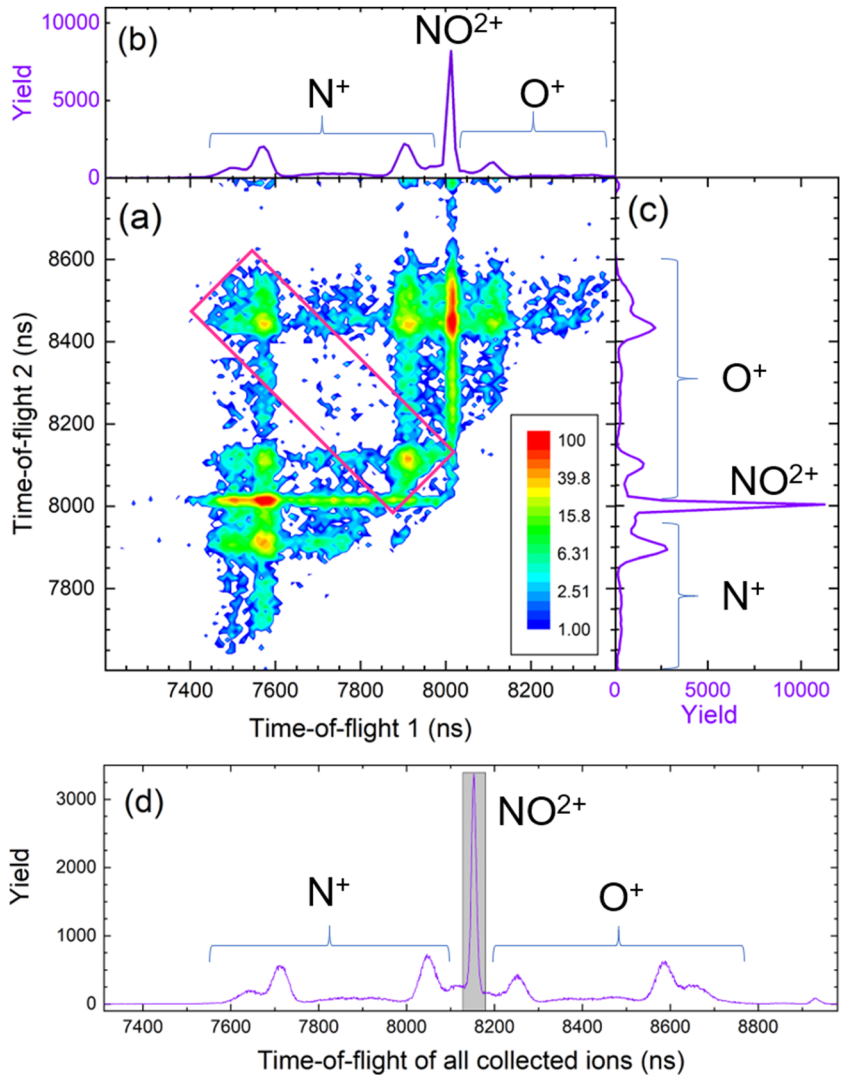

FIG. 3. One- and two-dimensional representations of coincidence-time-of-flight data of NO^{2+} dissociation. Panel (a) shows the coincidence yield (log scale) as a function of the TOF of the first and second fragments. The magenta box identifies $N^+ + O^+$ coincidences. Panels (b) and (c) show the yield vs TOF of the first and second fragments, respectively, integrated over the yield of the other fragment. Panel (d) shows the yield vs time-of-flight for all fragments. The shaded area in (d) indicates the region from which the NO^{2+} yield is determined. Panels (a)–(c) have their time resolution compressed by a factor of ten to control the size of the two-dimensional spectrum, while panel (d) shows higher 1 ns/channel time resolution. The data presented were obtained with FTL laser pulses at 0.04 mJ/pulse or approximately 5×10^{14} W/cm^2. The lack of events in the center of the coincidence stripe indicates a strong preference for the ions to be ejected along the polarization (TOF) direction. By rotating and projecting the events within the diagonal box shown in panel (a), the $P(E_k)$ distribution for the coincidence events may be evaluated from the time-difference between the ion-pairs.[68,69]

one ion is lost due to detection efficiencies less than one) can be subtracted.[68] A typical coincidence time-of-flight (CTOF) plot is shown in Fig. 3. The corrected $N^+ + O^+$ yield and the NO^{2+} yield from the same measurement, shown in Fig. 3, were used to derive the value of the control objective reported in Sec. III. As described later, the CTOF data can also be used to deduce the fragment dissociation energy.

Figure 3 shows a moderate number of purely random coincidences, such as $N^+ + NO^{2+}$. Experimentally, controlling these random coincidence rates is the most difficult part of the measurement, since the adaptive control loop requires a relatively high rate for feedback. Too high of a target gas pressure, however, can increase the random coincidence rate to a level that will produce spurious feedback. Balancing the overall ion production rate is important and in some cases can limit the effective dynamic range of the experiment. This can be partially avoided by starting the experiment at a higher gas pressure until the fitness values begin to "take off" and then stopping the experiment and reducing the gas pressure. The GA is then restarted from the preceding generation.

The second part of the postoptimization analysis is to obtain the momentum distribution, and therefore the E_k and angular distribution, of the dissociating fragments using VMI. Specifically, the N^+ and O^+ fragments produced by the optimally shaped and FTL laser pulses were measured using a VMI spectrometer.[58,62,64] While the VMI spectrometer is different from the Wiley-McLaren TOF spectrometer, the laser focusing optic is identical (f = 75 mm), and care is taken to reproduce the laser beam profile as closely as possible to the conditions of the CTOF measurement. To verify that this was achieved, we checked that the details of the TOF spectrum obtained using the VMI spectrometer, such as the ratio of the various ions, were the same as expected from earlier measurements with the TOF spectrometer. The TOF spectra could not be exactly matched,

25 September 2023 21:20:00

however, due to the differences in the TOF resolution between the two spectrometers and the different laser polarization direction relative to the TOF axis used in the two setups.

The raw two-dimensional VMI data are inverted to recover a slice through the center of the three-dimensional momentum distribution using a modified "onion-peeling" or "back-projection" algorithm as described by Rallis *et al.*[58] Several other methods[70–72] of performing the inverse-Abel transformation were also tested to ensure that any relevant features were not due to numerical artifacts associated with the inversion process.

The probability of dissociation as a function of kinetic energy release, $P(E_k)$, can also be evaluated from CTOF data[68,69] by using the difference in arrival times of the coincident N^+ and O^+ fragments, although the angular distribution cannot be measured as directly as with VMI. The two methods are complimentary, since the CTOF-generated $P(E_k)$ distribution can be correlated with $N^+ + O^+$ coincidences, while the VMI-derived $P(E_k)$ distribution measures all N^+ or, separately, all O^+ ions, including those from different charge states of the intermediate NO^{q+} ions.

For our two-stage Wiley-McLaren[65] time-of-flight (TOF) spectrometer, the kinetic energy release from dissociative ionization is

$$E_k = \frac{(V_2 - V_1)^2}{8md^2} q^2 \Delta t^2, \tag{1}$$

where V_2 and V_1 are the voltages on the extraction and acceleration meshes, respectively, d is the distance between the meshes, m and q are the mass and charge of the ion, and Δt is the time between the forward and backward traveling ions.[68] The associated probability of dissociation as a function of E_k is

$$P(E_k) = [t_{21}(E_k, 0^\circ) - t_{21}(E_k, 180^\circ)] \frac{dt_{21}}{dE_k} \frac{dY}{dt_{21}}, \tag{2}$$

where $t_{21}(E_k, 0^\circ)$ and $t_{21}(E_k, 180^\circ)$ (i.e., $\theta = 0^\circ$ and 180°) associated with the short-TOF fragment having initial velocity toward and away-from the recoil detector, respectively, are the maximum and minimum time differences, respectively. dY/dt_{21} is the numerical time derivative of the large time-difference side of the spectrum. The $P(E_k)$ distributions obtained with both VMI and CTOF methods are shown in Fig. 4, which reveals that the KER of the $N^+ + O^+$ channel falls within the 5–9 eV range.

In summary, the experimental procedure consists of two steps: (1) The optimization step in which the learning algorithm searches for a pulse shape guided by CTOF feedback and (2) the subsequent analysis step, in which multihit TOF spectra, VMI data, and SHG-FROG pulse measurements are recorded using the optimized laser pulses that are obtained in the first step.

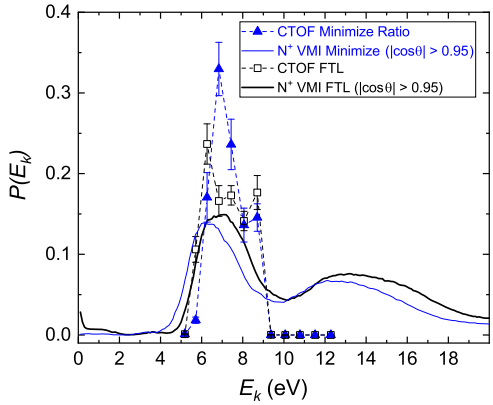

FIG. 4. The probability of dissociation, $P(E_k)$, as a function of E_k for FTL pulses (black) and pulses that minimize the $NO^{2+}/(N^+ + O^+)$ ratio (blue) at 0.04 mJ/pulse. The probabilities are obtained using two different methods. The symbols are a result of analysis of the CTOF data shown in Fig. 3 (as described in the text), while the solid lines represent the VMI data. Specifically, the solid lines are projections of the density plots shown in Figs. 7(a) and 7(b). The CTOF-derived probability unambiguously identifies the $N^+ + O^+$ coincidence channel, while the VMI-derived data have higher KER resolution but are recorded for all N^+ ions, i.e., including channels such as $N^+ + O$. Since the CTOF-data in Fig. 3 fall almost exclusively along the polarization direction, the VMI-derived data are restricted to $|\cos\theta| > 0.95$ for comparison.

III. RESULTS AND DISCUSSION

The $NO^{2+}/(N^+ + O^+)$ ratio changes with the pulse intensity, as shown in Fig. 5, for FTL pulses of about 40 fs FWHM in duration. As the intensity increases, the ratio of nondissociative to dissociative double ionization decreases, dropping from 4.0 at 2×10^{14} W/cm^2 to 0.23 at 7×10^{15} W/cm^2. The fact that the $NO^{2+}/(N^+ + O^+)$ ratio decreases as the intensity increases can be attributed to the fact that highly excited vibrational states of NO^{2+} ($v \geq 12$ for the electronic ground state) rapidly dissociate, and these states, including excited electronic states, are more readily populated at higher intensities. For this reason, the main control experiments were conducted at intensities between 5 and 8×10^{14} W/cm^2 for which the $NO^{2+}/(N^+ + O^+)$ ratio was near unity and simple intensity changes (i.e., "trivial control"[3]) might not have a dramatic impact on this ratio.

We did, however, examine the effectiveness of the control at higher pulse energies, in light of several suggestions in the literature that the behavior of NO might evolve as the intensity increases.[53,73] In these higher energy experiments, the $NO^{2+}/(N^+ + O^+)$ ratio could be enhanced by a factor of 3.9 over the result with a FTL pulse. Attempts to minimize the same ratio were quantitatively

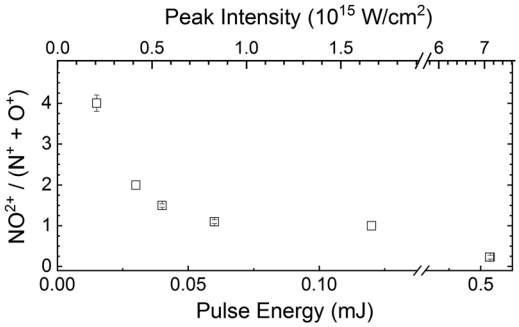

FIG. 5. The $NO^{2+}/(N^+ + O^+)$ ratio for 40 fs FWHM near-Fourier transform limited (FTL) pulses as a function of pulse energy. The corresponding intensity is shown on the upper axis. The error bars represent the statistical uncertainty including "lost fragment" and random coincidence corrections.

25 September 2023 21:20:00

TABLE I. The measured $NO^{2+}/(N^+ + O^+)$ ratio acquired with different pulse energies. The different columns represent the values obtained with FTL pulses as well as pulses optimized to maximize or minimize this ratio.

Pulse energy (mJ)	FTL ratio	Maximize ratio	Minimize ratio
0.015	4.0 ± 0.2		
0.03	2.0 ± 0.1		
0.04	1.50 ± 0.04	2.8 ± 0.9	0.80 ± 0.05
0.06	1.10 ± 0.05	13.8 ± 2.1	0.90 ± 0.03
0.06		6.0 ± 0.9	0.77 ± 0.04
0.12	1.0 ± 0.1		
0.52	0.23 ± 0.05	0.9 ± 0.2	0.0001 ± 0.0002
0.51	0.23 ± 0.10	0.7 ± 0.2	0.0005 ± 0.0004

more successful, with essentially all the NO^{2+} yield eliminated. The control results for all measured pulse energies are summarized in Table I.

The ability to decrease the $NO^{2+}/(N^+ + O^+)$ ratio with higher energy pulses is unsurprising, since all that is required is that the NO^{2+} yield be reduced. As the pulse energy increases, the laser-molecule interaction becomes more nonperturbative in character. As a result, there are many ways[21,74,75] the lower-lying NO^{2+} X $^2\Sigma^+$ vibrational population can be excited to dissociative levels, including nonresonant dynamic Stark shifts.[76,77] A signature that strong-field dynamics, such as the nonresonant dynamic Stark shifts, are dominant is the depletion of the ground state,[78] which we observe as a NO^{2+} yield that is consistent with zero.

On the surface, it would seem more surprising that the $NO^{2+}/(N^+ + O^+)$ ratio could be enhanced at these higher intensities. Some of this enhancement, however, can be explained by the range of intensities in the focal volume. While the $N^+ + O^+$ coincidence condition selects a certain intensity range from within the focal volume, the NO^{2+} yield need not arise from the same focal volume as the $N^+ + O^+$ ion-pairs. Thus, at peak intensities where the dissociative double ionization dominates, the NO^{2+} can still be produced by slightly lower intensity portions of the focal volume.

Another feature of the higher pulse energy experiments is the significant complexity of the optimized pulses, for both maximizing and minimizing $NO^{2+}/(N^+ + O^+)$. While it may be possible to unravel the mechanisms that occur in these complex pulse shapes at higher intensities,[26,27,37,44,79,80] attempting to understand the control mechanisms at lower pulse energies seems a more promising starting point. At pulse energies around 0.04–0.06 mJ, the $NO^{2+}/(N^+ + O^+)$ value is around one for the FTL pulses and neither the NO^{2+} nor $N^+ + O^+$ channels are near an appearance intensity threshold. This minimizes the possibility of control due to simple intensity changes. As shown in Table I, using pulse energies of 0.04 and 0.06 mJ to maximize the $NO^{2+}/(N^+ + O^+)$ ratio results in an increase by as much as 12.5 times the values obtained with a FTL pulse. Minimizing the same ratio results in a decrease of approximately 1.9 times the FTL value.

Figures 6(a) and 6(b) show the time-of-flight spectra for two specific trials we examine in detail. Optimizing the pulse shape to minimize the $NO^{2+}/(N^+ + O^+)$ ratio, as shown in Fig. 6(b), results in a TOF spectrum that appears very similar to the TOF spectrum

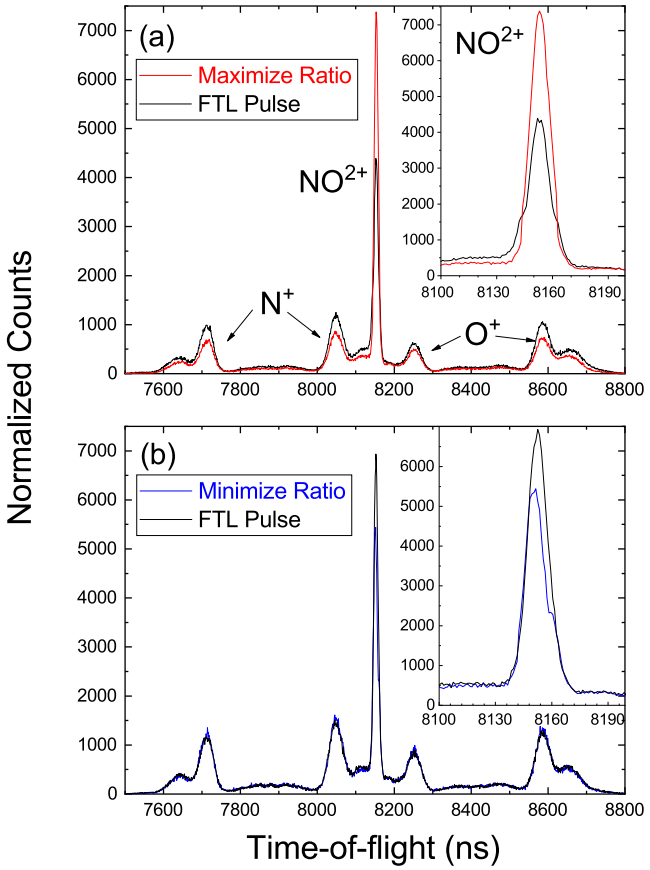

FIG. 6. Time-of-flight spectra of all ions in the relevant time window measured in association with (a) 0.06 mJ/pulse and (b) 0.04 mJ/pulse laser pulses. The narrow peak around 8150 ns is associated with NO^{2+} and is highlighted in each inset. The N^+ and O^+ fragments appear as "forward" (short TOF) and "backward" (long TOF) peaks. The highest energy N^+ (backward) and O^+ (forward) fragments overlap the NO^{2+} peak but should have little effect on our conclusions. In panel (a), the yield from pulses optimized to maximize the $NO^{2+}/(N^+ + O^+)$ ratio (red line) are compared to those measured with FTL pulses of the same energy (black line). Panel (b) is similar, but for the pulses optimized to minimize the same ratio (blue line). The number of counts are normalized to the number of laser shots in both panels.

obtained with an FTL pulse at the same energy, save for a reduction in the NO^{2+} yield shown in the inset. Closed-loop optimization with the aim of maximizing the $NO^{2+}/(N^+ + O^+)$ ratio, on the other hand, seems to enhance the amount of NO^{2+} and also slightly decrease the amount of dissociative double ionization, i.e., $N^+ + O^+$. We note that the data shown in Fig. 6 include all ions, similar to the time-of-flight data shown in Fig. 3(d), and thus, the value of the $NO^{2+}/(N^+ + O^+)$ ratio cannot be directly evaluated from this plot.

Before examining the changes that occur when the optimized pulses are used, it is worthwhile to examine the results acquired with the FTL pulses. Figure 7 shows the N^+ and O^+ VMI data, corresponding to the FTL-TOF spectra shown in Fig. 6(b), as a function of E_k and the cosine of the angle between the N^+ fragment

25 September 2023 21:20:00

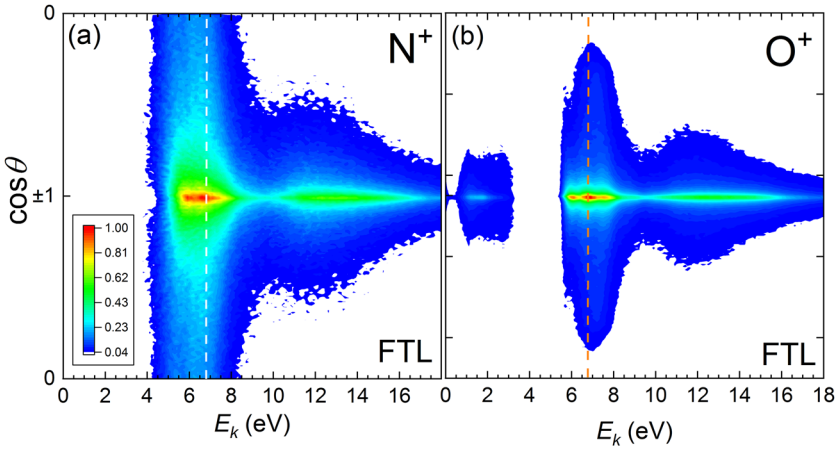

FIG. 7. The yield of N^+ (a) and O^+ (b) photofragments as a function of E_k and $\cos\theta$, where θ is the angle between the N^+ fragment velocity and the laser polarization direction. These plots are obtained by transforming the VMI data shown in Fig. 2(c). Panel (a) shows N^+ fragments produced using FTL pulses at 0.04 mJ/pulse or approximately 5×10^{14} W/cm^2, while panel (b) shows O^+ fragments at the same pulse conditions. The dotted lines at 6.8 eV in each panel represent the peak E_k value, and the angular distributions along those lines are shown in Fig. 9.

velocity and the laser polarization axis, $\cos\theta$. The same data are presented in Fig. 2(c) as a momentum plot, but the representation in Fig. 7 is often more useful for interpretation. Figure 4 shows $P(E_k)$ of the $N^+ + O^+$ ion-pair events unambiguously identified by the CTOF method. This $P(E_k)$ spectrum has two maxima, at 6.3 eV and at 8.7 eV. The VMI data (Fig. 7) have higher E_k resolution, but are not restricted to $N^+ + O^+$ ion-pair events. Since the CTOF data shown in Fig. 3(a) indicate that the $N^+ + O^+$ ion-pairs are strongly aligned with the laser polarization direction, we can select the aligned portion of the $E_k - \cos\theta$ plots (Fig. 7) in order to compare the CTOF- and VMI-based measurements of $P(E_k)$. Slices from Figs. 7(a) and 7(b) with $|\cos\theta| > 0.98$ show the yield in a 5–9 eV region, as illustrated in Fig. 8, which is similar to the region of large $P(E_k)$ in Fig. 4. The most likely E_k value from these VMI-derived measurements is at about 6.8 eV. The $P(E_k)$ distributions derived from the aligned

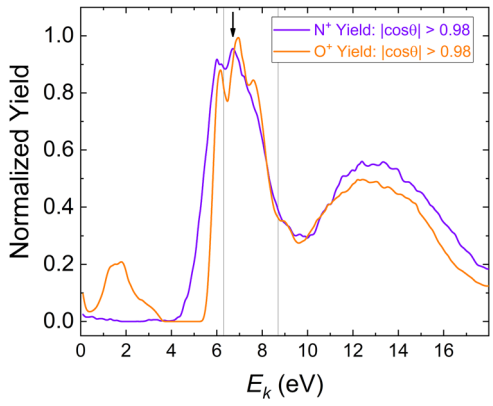

FIG. 8. The yield of N^+ (violet) and O^+ (orange) as a function of E_k for $|\cos\theta| \geq 0.98$. The peaks around 13 eV are due to NO^{3+} (or higher charge state) dissociation. CTOF measurements identify the 5–9 eV region as the location of the $N^+ + O^+$ ion-pairs. The approximate peak of the VMI data at 6.8 eV is indicated by an arrow, while the vertical lines label the locations of the 6.3 eV and 8.7 eV peaks in the $P(E_k)$ distribution shown in Fig. 4.

N^+ and O^+ fragments (shown in Fig. 8) have different features. Furthermore, these details also differ from the $P(E_k)$ distribution determined from the $N^+ + O^+$ ion-pair distribution shown in Fig. 4. The different $P(E_k)$ distributions indicate that the VMI measurement is probably dominated by dissociative single ionization leading to $N^+ + O$ or $N + O^+$, since $N^+ + O^+$ ion-pairs produced from the dissociation of NO^{2+} would have the same momentum for the N^+ and O^+ fragments.

The angular distribution of the features in the $P(E_k)$ distributions, illustrated in Fig. 9, confirms that the $N^+ + O^+$ ion-pairs are not the dominant contributor to the VMI $E_k - \cos\theta$ data shown in Fig. 7. When excited with a linearly polarized laser pulse, electric dipole transitions between the initial and final states with the same angular momentum, $\Delta\Lambda = 0$, are expected to have a $\cos^{2n}\theta$ angular distribution (where n is the number of photons), while for a $\Delta\Lambda = 1$ transition, the angular distribution should follow a $\sin^{2n}\theta$ distribution.[60,61,81] A transition accessing an intermediate state so as to make a parallel transition ($\Delta\Lambda = 0$) followed by a perpendicular transition ($\Delta\Lambda = 1$) or vice versa should be fit by a function of the form $\cos^{2n}\theta \sin^{2m}\theta$. The angular distributions for both the N^+ and O^+ fragments with E_k between 6.75 and 6.85 eV, shown in Figs. 9(c) and 9(d), seem to contain multiple components. Examining the angular distributions for E_k between 6.25 and 6.35 eV and between 8.65 and 8.75 eV, corresponding to the peaks in the CTOF-E_k data obtained with the FTL pulse (see Fig. 4) and shown in Figs. 9(a) and 9(b) and Figs. 9(e) and 9(f), yields the same conclusion. For all three E_k regions, the main parallel component of the angular distribution is much broader in the N^+ case, fitting to $\cos^6\theta$, while the narrower O^+ distribution is best fit with $\cos^{16}\theta$ at E_k between 6.75 and 6.85 eV and $\cos^{18}\theta$ in the other two cases. Thus, even for fragments ejected nearly along the laser polarization, the angular distributions associated with the N^+, O^+, and $N^+ + O^+$ ion-pairs (see Fig. 3) are quite different.

Since the VMI-derived data contain a significant amount of $N^+ + O$ and $N + O^+$ fragments in addition to the $N^+ + O^+$ channel of interest, can we use the CTOF-derived data to better understand the multiple ionization process that leads to NO^{2+}? Multiple ionization of diatomic molecules has been studied in many experiments, and there are several possible routes for the transition

25 September 2023 21:20:00

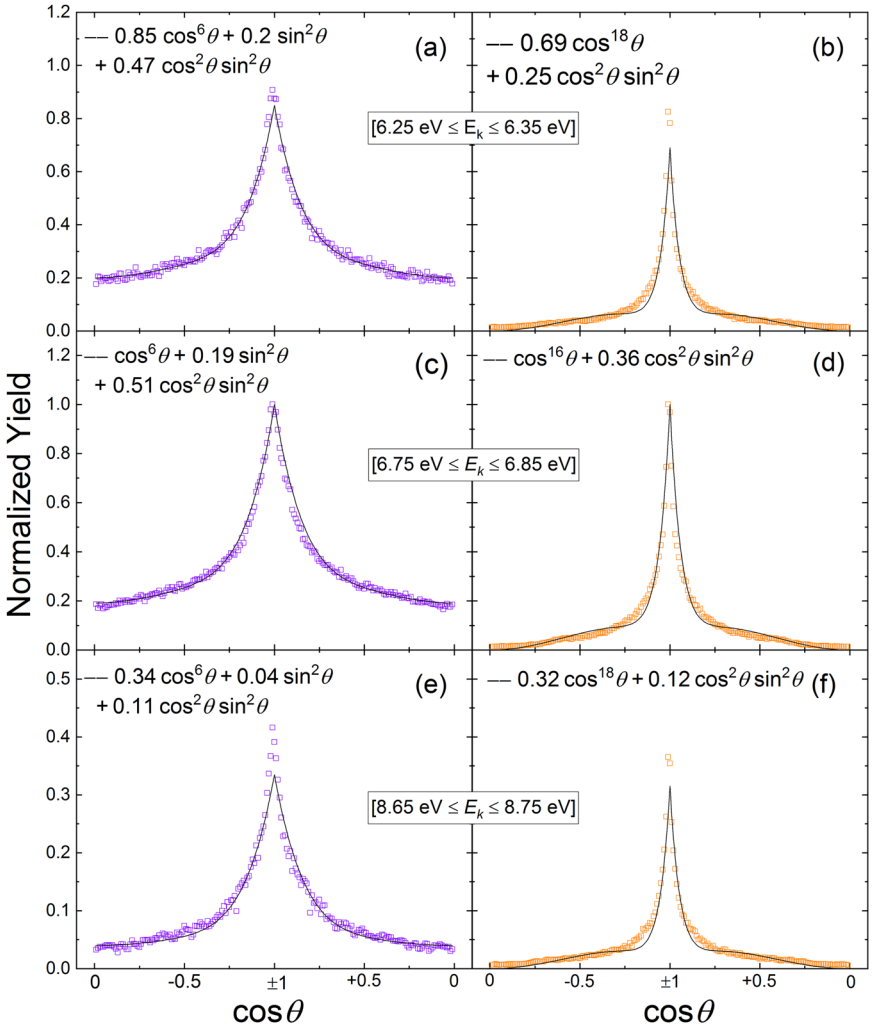

FIG. 9. The normalized yield of N^+ (left column) and O^+ (right column) as a function of cos θ. The slices through the data shown in Fig. 7 are made at three locations: ($6.25 \le E_k \le 6.35$), the first peak in the $P(E_k)$ distribution from Fig. 4 [panels (a) and (b)], ($6.75 \le E_k \le 6.85$), the peak of the VMI yield as indicated by the line in Fig. 7 [panels (c) and (d)], and ($8.65 \le E_k \le 8.75$), the second peak in the $P(E_k)$ distribution from Fig. 4 [panels (e) and (f)]. The fits shown are of the form $A\cos^{2n}\theta + B\sin^{2m}\theta + C\cos^{2k}\theta\sin^{2l}\theta$ for the N^+ fragments and $A\cos^{2n}\theta + C\cos^{2k}\theta\sin^{2l}\theta$ for the O^+ fragments.

from neutral NO to NO^+ and ultimately NO^{2+}: Both direct ionization[82,83] and electron rescattering[83–87] (also called nonsequential or recollision ionization) occur near the equilibrium internuclear distance, R_e, since the nuclei do not have much time to respond to the laser field in either case. The recolliding electron can carry considerable energy, up to $3.17U_p$, where U_p is the pondermotive energy,[84] potentially leading to electronic excitation of the parent ion as well as multiple ionization.[88] Various Coulomb explosion[89–96] and enhanced ionization mechanisms[96–109] provide a link between E_k and the internuclear distance at which ionization occurs (often called the critical internuclear distance, R_c). These models, however, work best for molecules that have dissociative states with purely repulsive potential energy curves and are not easily applied to the metastable potential energy curves of NO^{2+}, which are illustrated in Fig. 1.

A simple application of the Coulomb explosion model, $E_k = 1/R_e$, gives an E_k value that is larger than the measured, while applications of the enhanced ionization models[109] lead to lower than the observed E_k values at very large R_c. While it is not surprising that these models do not work well for NO, the upper and lower limits they supply for E_k suggest some sort of intermediate behavior with the ionization occurring between R_e and R_c. One such possibility would be a stairstep ionization process[110] in which the molecule stretches before each sequential ionization step.

Previous experimental studies of laser-induced ionization and dissociation of neutral NO leading to $N^+ + O^+$ fragments[73,111–116] have generally not employed coincidence measurements. Most of these studies suggest that the N^+ and O^+ fragments are produced indirectly, either by first dissociating NO and ionizing one or more fragments[111] or by population of another intermediate state of NO^+ or NO^{2+}. Furthermore, the measured $P(E_k)$ of the $N^+ + O$ and $N + O^+$ dissociation channels of NO^+ (see Fig. 8) is consistent with ionization at $R_e < R < R_c$.

The angular distributions of the ionization process can also help clarify the underlying dynamics. Given the duration of the pulses used in these experiments, both geometrical and

25 September 2023 21:20:00

dynamic molecular alignment must be considered.[117–122] Molecular Ammosov-Delone-Krainov (MO-ADK) theory,[123] which employs the principle of geometrical alignment, predicts that the angular distribution should reflect the symmetry of the most loosely bound electron of the molecule. For neutral NO, the HOMO has π_g symmetry, and thus, MO-ADK would suggest that the maximum ionization rate occurs at about 40° away from the polarization axis. As Voss and co-workers have shown, at higher intensities (near 1×10^{15} W/cm^2), this effect becomes smaller due to dynamic alignment,[124] including postpulse alignment.[121] While the intensity here is not as high, the ionization potential of NO is low (9.264 eV), and therefore, the initial ionization leading to NO^{2+} may be more peaked along the polarization direction than the MO-ADK prediction.

Intense laser interactions with beams of NO cations[110] and dications[53] produce angular distributions of fragments that can help clarify the current results from neutral NO targets. In the ion-beam experiments, the distributions of NO^+ and NO^{2+} ions in the laser focus are known to be isotropic.[53,110] In the NO^{2+} beam measurement, the subsequent laser-induced dissociation leads to perpendicular transitions at intensities comparable to the current experiment. Thus, we can conclude that the laser-induced NO → NO^{2+} process does not produce an isotropic distribution of NO^{2+} ions, since these perpendicular transitions are not dominant in the current experiment, as shown in Figs. 3(a), 7, and 9. Stated another way, we know that NO^{2+} tends to dissociate more easily when it is perpendicular to the laser pulse,[53] but we do not observe that angular behavior in our data. Instead, we see more ion-pairs emitted along the laser polarization. Thus, we infer that the initial NO → NO^{2+} ionization is not isotropic and is more probable for molecules that have $\cos\theta = \pm 1$.

In general, the angular distribution we observe in Fig. 7 resembles the observations of Gaire *et al.*[110] for single ionization of a NO^+ beam leading to $N^+ + O^+$ ion-pairs. In both that work[110] and in the current experiment, the angular distribution is predominantly aligned along the laser polarization but is wider than expected for a purely parallel transition. The presence of both perpendicular and parallel ionization routes suggests at least some contribution from stepwise processes in which the transition from NO → NO^+ and the subsequent NO^+ → NO^{2+} step can both influence the angular distributions even before the final $NO^{2+} \rightarrow N^+ + O^+$ dissociation.

Since the minimum of the X $^2\Sigma^+$ electronic state of NO^{2+} is 1.6 eV lower in energy than the minimum of the A $^2\Pi$ state, we can assume that the initial ionization preferentially populates the X $^2\Sigma^+$ electronic state, even though the Franck-Condon overlap between the neutral NO ground state and the NO^{2+} X $^2\Sigma^+$ state is similar to the Franck-Condon overlap between the neutral NO and the NO^{2+} A $^2\Pi$ state (see Fig. 1). This assumption does not mean that we can exclude population of other states through more complex mechanisms, for example, stepping through the monocation states and stretching before ionization of the second electron. Under the assumption that the X $^2\Sigma^+$ is preferentially populated, we can exclude a number of possible routes to dissociative double-ionization based on the observed angular distribution of the $N^+ + O^+$ ion-pairs shown in Fig. 3. While the observed $P(E_k)$ is consistent with what is expected for several one-photon NO^{2+} X $^2\Sigma^+ \rightarrow$ A $^2\Pi$ transitions, such as

$$\mathrm{X}\,^2\Sigma^+(v=4) \rightarrow \mathrm{A}\,^2\Pi(v=7)\ (E_k \approx 6.5\ \mathrm{eV}),$$
$$\mathrm{X}\,^2\Sigma^+(v=6) \rightarrow \mathrm{A}\,^2\Pi(v_{cont})\ (E_k \approx 6.9\ \mathrm{eV}),$$
$$\mathrm{X}\,^2\Sigma^+(v=7) \rightarrow \mathrm{A}\,^2\Pi(v_{cont})\ (E_k \approx 7.3\ \mathrm{eV}).$$

X $^2\Sigma^+ \rightarrow$ A $^2\Pi$ transitions have $\Delta\Lambda = 1$, and therefore, the breakup should be perpendicular to the laser polarization,[60,61,81] or at least show a $\cos^{2n}\theta \sin^{2m}\theta$ distribution if the initial NO → NO^{2+} X $^2\Sigma^+$ ionization step is aligned along the laser polarization. The X $^2\Sigma^+$ → B $^2\Sigma^+$ are $\Delta\Lambda = 0$ transitions that can result in similar E_k values, which are consistent with the current measurements, but this requires either two or three more photons than the one-photon X $^2\Sigma^+ \rightarrow$ A $^2\Pi$ transitions and, in some cases, needs to start in a higher vibrational level of the X $^2\Sigma^+$ state.

Energetically, the lower 6.3 or 6.8 eV peak in the measured E_k distribution would be consistent with a near-vertical transition from the neutral ground state to the NO^{2+} ground state followed by three-photon X $^2\Sigma^+$ ($v = v_i$) → X $^2\Sigma^+$ ($v = v_f$) vibrational excitation leading to dissociation, where v_i and v_f are the initial and final vibrational states, respectively. In other words, the leading portion of the pulse removes the electrons, without stretching the molecule much, and the role of any additional photons is to shift the vibrational population from a bound state to a dissociative state via a permanent dipole transition. Calculations of the field-free Franck-Condon overlap factors, displayed in Fig. 1(b), show that direct vertical transitions to NO^{2+} X $^2\Sigma^+$ from the neutral NO ground state predominantly populate the $v = 0$ through $v = 5$ levels of NO^{2+} (peaked at $v = 1$), consistent with the observed E_k and X $^2\Sigma^+ \rightarrow$ X $^2\Sigma^+$ transitions. Jochim *et al.*[53] have shown that X $^2\Sigma^+ \rightarrow$ X $^2\Sigma^+$ permanent dipole transitions leading to vibrational excitation and dissociation into $N^+ + O^+$ are more likely than competing channels over the range of E_k values discussed here.

The secondary peak at $E_k = 8.7$ eV in the $P(E_k)$ distribution (shown in Fig. 4) supports the interpretation presented in the previous paragraph, since permanent dipole transitions dominate over X $^2\Sigma^+ \rightarrow$ B $^2\Sigma^+$ transitions leading to $N^+ + O^+$ fragments with $E_k > 8$ eV.[53] Besides the calculations[53] showing the dominance of the X $^2\Sigma^+ \rightarrow$ X $^2\Sigma^+$ over the X $^2\Sigma^+ \rightarrow$ B $^2\Sigma^+$ transitions due to the smaller number of required photons and the relative magnitudes of the couplings between these states, resonance-enhanced multiphoton ionization may further bolster this pathway relative to direct nonresonant multiphoton ionization.[103,105]

Thus, given the prevalence of the X $^2\Sigma^+ \rightarrow$ X $^2\Sigma^+$ transitions over the X $^2\Sigma^+ \rightarrow$ B $^2\Sigma^+$ transitions and a photofragment angular distribution that seems to make one-photon NO^{2+} X $^2\Sigma^+$ → A $^2\Pi$ transitions unlikely, we believe that the FTL-driven dissociative double ionization process likely involves ionization to a low-lying vibrational state of NO^{2+} followed by X $^2\Sigma^+ \rightarrow$ X $^2\Sigma^+$ vibrational excitation leading to dissociation aligned with the laser polarization with the observed E_k values.

What role, then, does the optimized pulse shape play in enhancing or suppressing the $NO^{2+}/(N^+ + O^+)$ ratio? Examining the suppression case first, we note that the optimized TOF spectrum, shown by the blue line of Fig. 6(b), is nearly identical to the TOF spectrum obtained with the FTL pulse (black line), except for the region of the NO^{2+} events. The optimized pulse seems to keep the TOF yield of the photofragment distributions largely unchanged while reducing the yield of the nondissociative NO^{2+} ions. This is supported by the

25 September 2023 21:20:00

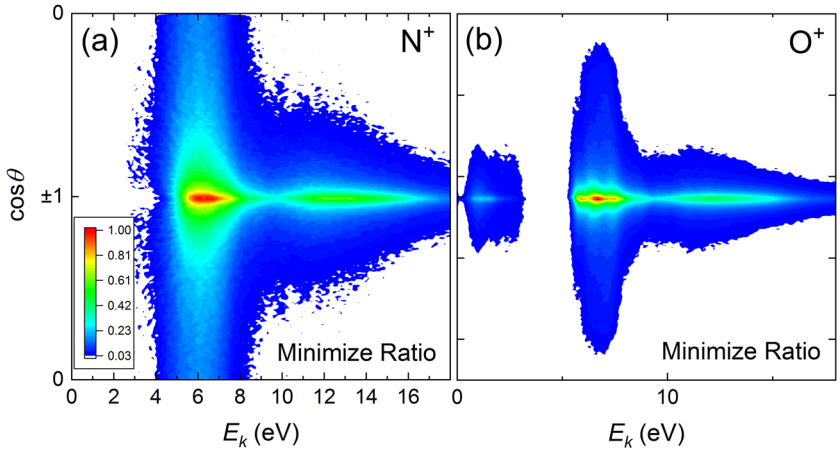

FIG. 10. The yield of N^+ (a) and O^+ (b) as a function of E_k and $\cos\theta$. (a) shows N^+ fragments produced using pulses that minimize the $NO^{2+}/(N^+ + O^+)$ ratio at 0.04 mJ/pulse ($\sim 5 \times 10^{14}$ W/cm^2). (b) shows O^+ fragments produced by the same optimized pulse. Both distributions are nearly identical to those shown in Fig. 7.

$E_k - \cos\theta$ distributions of the N^+ and O^+ ions produced with optimized pulses shown in Fig. 10, which also appear nearly identical to the FTL-generated $E_k - \cos\theta$ distributions shown in Fig. 7.

The measured SHG FROG traces of the optimized pulse that minimized the $NO^{2+}/(N^+ + O^+)$ ratio are shown in Fig. 11. This pulse has a FWHM of 65 fs, or about 60% wider than the FTL pulse. While the spectral intensity shows some modulation, neither the spectral nor temporal phases show much variation over the main intensity of the pulse. Thus, the optimized pulse seems to be somewhat longer in duration than a FTL pulse but does not appear to have many other significant features.

Since there are no significant changes to the photofragment distributions between the optimized and FTL pulse, the control by the optimized pulse can be interpreted as moving NO^{2+} population to higher vibrational states by allowing the molecule more time to stretch in the field before the last transition occurs. As shown by the Franck-Condon region in Fig. 1, when R increases, the probability of accessing higher vibrational levels of the $X\,^2\Sigma^+$ state increases. Support for this interpretation is provided in Fig. 4, which shows that the optimized pulses increase the number of $N^+ + O^+$ coincidence events at around $E_k = 7$ eV. If the penultimate step in the process drives the population to a higher $X\,^2\Sigma^+$ vibrational level than the

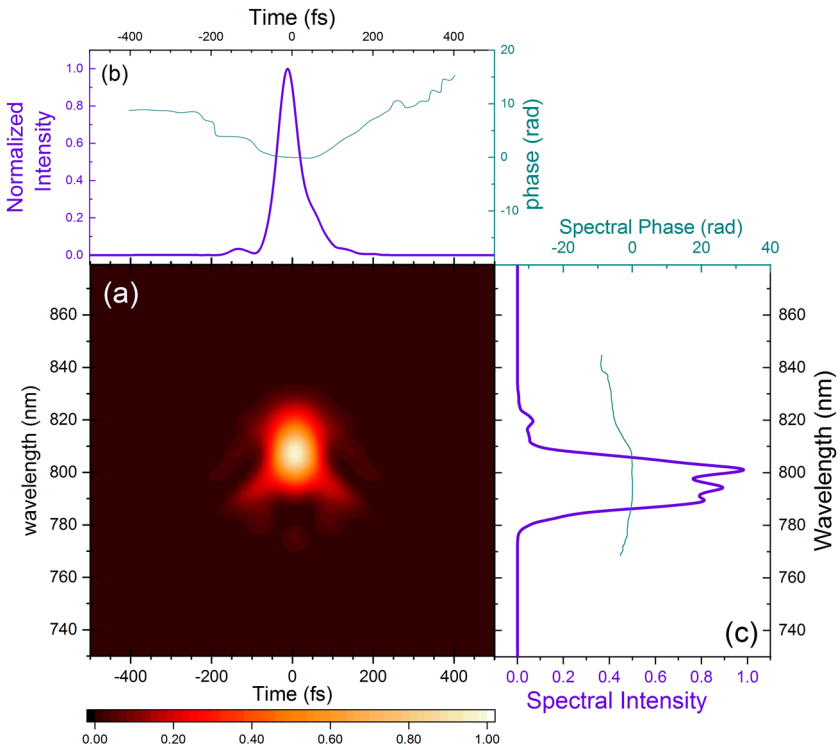

FIG. 11. Measured SHG FROG[63] trace (a) of the laser pulse optimized to minimize the $NO^{2+}/(N^+ + O^+)$ ratio at 0.04 mJ/pulse. The linear color scale is normalized, so the peak signal is 1.0. (b) The associated temporal intensity (thick purple) and phase (thin cyan) of the laser pulse. The FWHM of the pulse in intensity is 65 fs. (c) The spectral intensity (thick purple) and phase (thin cyan) of the laser pulse. The measured phase values are not meaningful at low intensities.

25 September 2023 21:20:00

FTL pulse, then the final step could land the same population in the dissociative region, with E_k consistent with the values that are enhanced in Fig. 4. In this explanation, the dissociation into $N^+ + O^+$ channels moves through the same pathways as when the FTL pulse is present, thereby explaining why the data in Figs. 7 and 10 are nearly identical, but the small shift in vibrational population depletes the bound NO^{2+} population, reducing the overall $NO^{2+}/(N^+ + O^+)$ ratio.

While this explanation seems fairly simple, lengthening the pulse to minimize the $NO^{2+}/(N^+ + O^+)$ ratio is the opposite of the "trivial" control behavior that would be predicted from the results shown in Fig. 5. Roughly extrapolating from Fig. 5, lengthening the pulse by 60% reduces the intensity of the 0.04 mJ/pulse to 3×10^{14} W/cm^2, which approximately doubles the $NO^{2+}/(N^+ + O^+)$ ratio. The longer pulse duration, then, is able to reduce the population of long-lived NO^{2+} even though the lower intensity should increase that same population. This indicates that the pulse duration effect on the vibrational population might be quite significant. On the other hand, the search algorithm had freedom to modulate the phase and extend the pulse duration further but did not choose this path, which may indicate that limiting the intensity eventually starts to increase the $NO^{2+}/(N^+ + O^+)$ ratio again. All three optimization trials in this pulse energy range (0.04 mJ/pulse and 0.06 mJ/pulse, see Table I) resulted in pulse characteristics similar to the pulse shown in Fig. 11.

As Table I details, the $NO^{2+}/(N^+ + O^+)$ ratio has also been increased by as much as a factor of 12.5 times over the value acquired with the FTL pulse using CTOF-based feedback. The comparison of the TOF spectra obtained with the 0.06 mJ/pulse FTL (~8×10^{14} W/cm^2) and optimized laser pulses is shown in Fig. 6(a). As noted previously, the two distinguishing features of this TOF measurement are the enhancement of the NO^{2+} yield and the smaller, but still notable, suppression of the N^+ and O^+ fragments, especially those with lower E_k.

The FROG trace of the optimized pulse that maximizes the $NO^{2+}/(N^+ + O^+)$ ratio is shown in Fig. 12. Unlike the pulse that minimizes the $NO^{2+}/(N^+ + O^+)$ ratio, the present pulse has an interesting structure in both the temporal and spectral domains. The main feature seems to be the two-pulse structure in the time domain. These two pulses are separated by about 151 fs. The FWHM of the individual peaks (88 and 69 fs) is similar to the width of the pulse that manipulated the vibrational population in the trials that minimized the $NO^{2+}/(N^+ + O^+)$ ratio. Thus, looking for a similar shift in vibrational population here seems reasonable, although we are now seeking to enhance, rather than suppress, the population of long-lived NO^{2+} states.

Some further information may be provided by the $P(E_k)$ distribution evaluated from the CTOF data, shown in Fig. 13 for the pulse that maximizes the $NO^{2+}/(N^+ + O^+)$ ratio and the FTL pulse at the same energy. The $P(E_k)$ values for the optimized pulse are lower than the FTL pulse up until $E_k \approx 6.5$ eV, which is consistent with the differences in the fragment yield observed in Fig. 6(a). This reduction of lower-E_k $N^+ + O^+$ fragments may indicate that the population has shifted to bound NO^{2+} vibrational levels.

The $E_k - \cos\theta$ distributions obtained by VMI measurements of N^+ or O^+ fragments for the laser pulses that maximized the $NO^{2+}/(N^+ + O^+)$ ratio are shown in Fig. 14. These photofragments are strongly peaked along the laser polarization, as shown in Fig. 15. While the bulk of the O^+ photofragment $E_k - \cos\theta$ distributions [Figs. 14(b) and 14(d)] are unchanged by the switch from

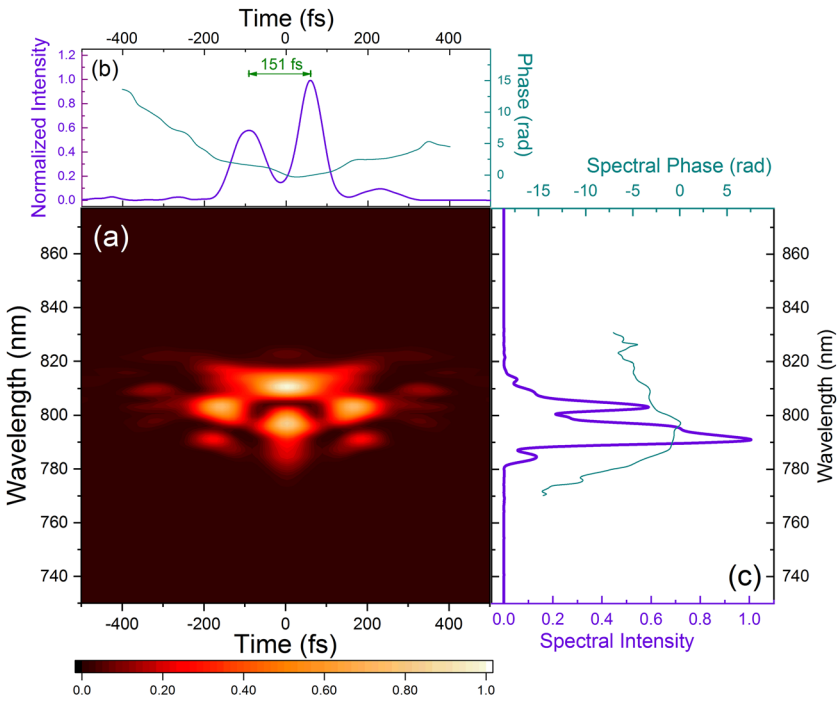

FIG. 12. Measured SHG FROG[63] trace (a) of the laser pulse optimized to maximize the $NO^{2+}/(N^+ + O^+)$ ratio at 0.06 mJ/pulse. The linear color scale is normalized, so the peak signal is 1.0. (b) The associated temporal intensity (thick purple) and phase (thin cyan) of the laser pulse. The centers of the two pulses are separated by 151 fs, with the earlier (left) pulse having 88 fs FWHM and the later (right) pulse having 69 fs FWHM. (c) The spectral intensity (thick purple) and phase (thin cyan) of the laser pulse.

25 September 2023 21:20:00

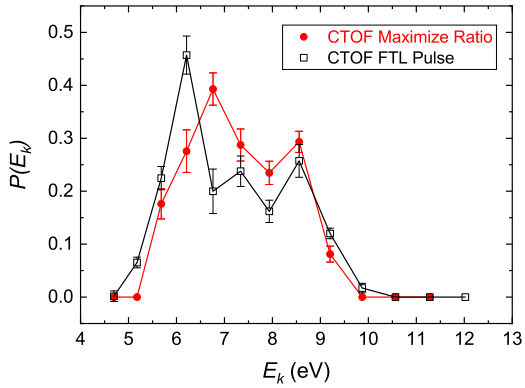

FIG. 13. The probability of dissociation, $P(E_k)$, as a function of E_k for FTL pulses (black) and for pulses that maximize the $NO^{2+}/(N^+ + O^+)$ ratio (red) at 0.06 mJ/pulse. The $P(E_k)$ distribution is derived from the CTOF data similar to that shown in Fig. 3 as described in the text. At lower E_k, the optimized pulse seems less likely to produce $N^+ + O^+$ ion pairs, in agreement with the TOF data shown in Fig. 6(a).

the FTL to the optimized pulses and have almost identical angular distributions in Fig. 15(b), there are some differences between the N^+ photofragment $E_k - \cos\theta$ distributions shown in Figs. 14(a) and 14(c). The optimized pulse tends to produce N^+ fragments with slightly lower E_k values than the FTL pulse. This is the opposite of the observation made from the CTOF-derived E_k data in Fig. 13, which showed that the FTL pulses were more likely to produce $N^+ + O^+$ ion pairs for $E_k \leq 6.5$ eV. Thus, the population of aligned N^+ photofragments near $E_k = 6$ eV evaluated from the VMI data must not originate from NO^{2+}, but instead come from a different parent ion, such as NO^+ dissociating into $N^+ + O$. The possibility of NO^{3+} dissociating into $(N^+ + O^{2+})$ with $E_k \sim 6$ eV is less likely since triple ionization requires increased laser intensity, and the resulting dissociation is expected to lead to larger E_k. For $NO^{3+} \rightarrow (N^+ + O^{2+})$, $E_k = 2/R_e \gg 6$ eV within the approximation of the Coulomb explosion model.

For the trials minimizing the $NO^{2+}/(N^+ + O^+)$ ratio, we developed the hypothesis that the increase in pulse duration (shown in Fig. 11) compared to the FTL pulse allowed higher vibrational states of NO^{2+} to be populated. Consistency would mean that the similar-in-duration first pulse in the sequence shown in the FROG trace of Fig. 12 must have much the same effect as the longer duration pulse that minimizes the $NO^{2+}/(N^+ + O^+)$ ratio even though the aim of this trial is to maximize the $NO^{2+}/(N^+ + O^+)$ ratio. One difference between the pulses optimized for minimization and maximization of the ratio, however, is that the maximizing pulse should have lower intensity than the minimization pulse measured in Fig. 11 since the pulse energy in Fig. 12 is split between two subpulses. An explanation for the utility of pulse characteristics of the maximization trial is that the first pulse populates higher vibrational states of NO^+ than a

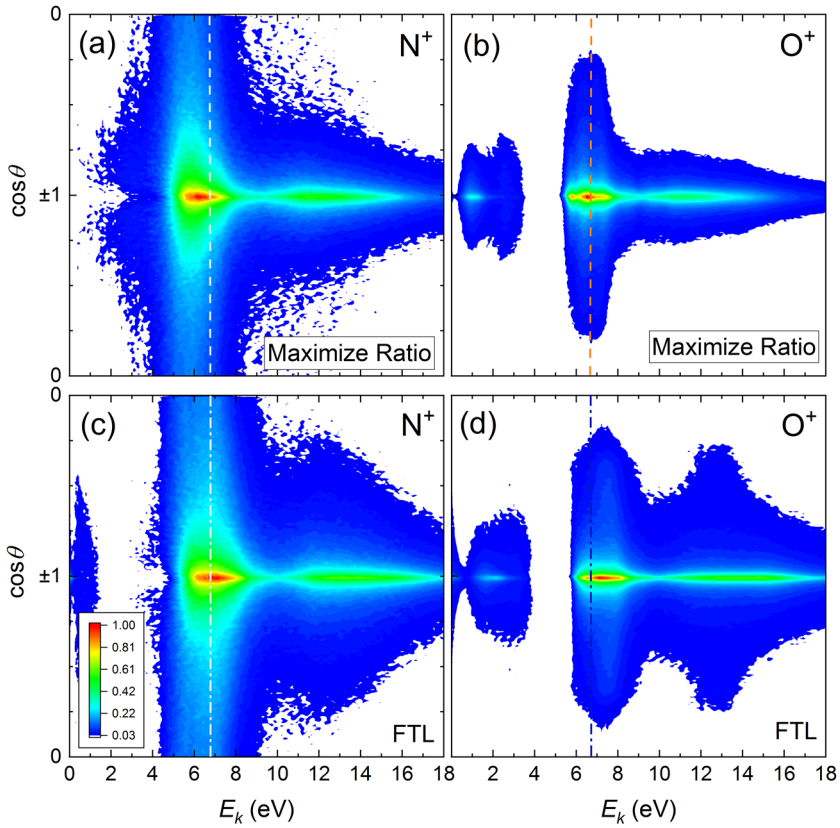

FIG. 14. Yields of N^+ and O^+ fragments as a function of E_k and $\cos\theta$. (a) N^+ fragments produced by the laser pulses optimized to maximize the $NO^{2+}/(N^+ + O^+)$ ratio at 0.06 mJ/pulse shown in Fig. 12. (b) O^+ fragments produced by the same laser pulse. (c) N^+ fragments produced by the FTL laser pulses at 0.06 mJ/pulse, equivalent to $\sim 8 \times 10^{14}$ W/cm^2. (d) O^+ fragments produced by the same FTL laser pulses. The dotted lines in each panel at $E_k = 6.7$ eV represent cuts used to produce the angular distributions shown in Fig. 15.

25 September 2023 21:20:00

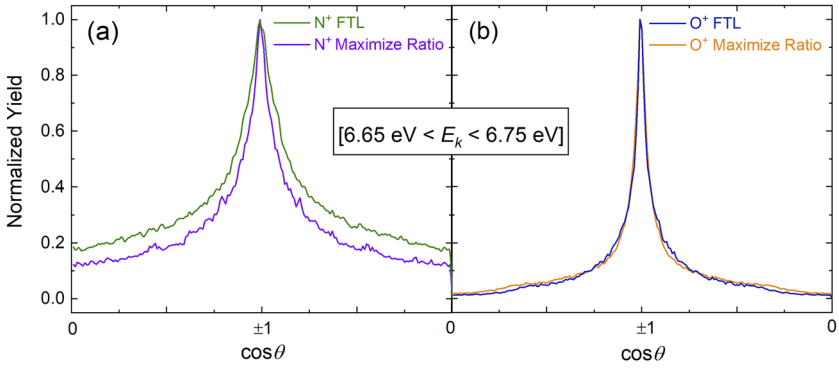

FIG. 15. (a) Angular distributions of N^+ photofragments, integrated over (6.65 eV ≤ E_k ≤ 6.75 eV), produced by pulses optimized to maximize the $NO^{2+}/(N^+ + O^+)$ ratio at 0.06 mJ/pulse (violet) and by FTL pulses of the same energy (olive), equivalent to ~8 × 10^{14} W/cm^2. (b) Angular distributions of O^+ photofragments, also integrated over (6.65 eV ≤ E_k ≤ 6.75 eV), produced by pulses optimized to maximize the $NO^{2+}/(N^+ + O^+)$ ratio at 0.06 mJ/pulse (orange) and by the FTL pulses of the same energy (blue). The slice around E_k = 6.7 eV chosen to examine the angular distributions matches the peak of the measured $P(E_k)$ distribution shown in Fig. 13. As in Fig. 9, the O^+ angular distributions are more strongly peaked than the N^+ fragments.

corresponding FTL pulse, leading to dissociation of the NO^+ cation by the secondary pulse rather than a second sequential ionization step. These dissociation channels, however, would be quite different than the E_k ~ 1–2 eV $NO^+ \rightarrow N^+ + O$ dissociations observed by Gaire *et al.*[110] for shorter pulses. The E_k − cos θ distribution in Fig. 14(a) indicates the presence of $N^+ + O$ fragments [absent from the CTOF-derived $P(E_k)$ distribution shown in Fig. 13], which are fairly strongly peaked along the laser polarization direction [see Fig. 15(a)].

To fit this single-ionization followed by dissociation understanding of the double-pulse structure of Fig. 12, we should be able to identify parallel transitions between a bound vibrational state of NO^+ and a dissociative state of NO^+ leading to N^+ fragments with E_k ~ 6 eV. Two potential transitions that match these criteria are displayed in Fig. 16, which shows (at least in the field-free picture) that eight photon, ΔΛ = 0 transitions from the v = 8 state of the NO^+ X $^1\Sigma^+$ ground electronic state would lead to the B $^1\Sigma^+$ state and dissociate with E_k ~ 6 eV. A similar seven photon transition from v = 13 also leads to the B $^1\Sigma^+$ state and has nearly the same E_k.

These transitions leading to dissociation of NO^+ could explain some of the "missing" $N^+ + O^+$ ion pairs in Fig. 13. With a more intense pulse, the pathway leading to bound vibrational states of the NO^{2+} ground electronic state and subsequent dissociation via X $^2\Sigma^+ \rightarrow$ X $^2\Sigma^+$ permanent dipole transitions would be open. In lowering the overall pulse intensity by forming a double-pulse structure, the maximization pulse avoids production of $N^+ + O^+$ ion pairs by enhancing a competing transition to $NO^+ \rightarrow N^+ + O$. Since the adaptive search uses coincidence-based feedback, the $NO^+ \rightarrow N^+ + O$ dissociation does not contribute to the fitness calculation, while the avoided $N^+ + O^+$ coincidence events would otherwise diminish the $NO^{2+}/(N^+ + O^+)$ ratio. This outcome would also explain why the N^+ E_k − cos θ distributions are different for the optimized and FTL pulses in Figs. 14(a) and 14(c), while the O^+ fragment distributions shown in Figs. 14(b) and 14(d) are more similar to each other, since the $N + O^+$ states are not involved in this scheme.

An additional attribute of the delayed second pulse shown in Fig. 12 is that the 150 fs delay between the first and second pulses gives the NO^+ vibrational wave packets time to evolve toward their equilibrium distance. Ionization near the NO^+ equilibrium would tend to populate lower vibrational levels of NO^{2+}, accounting for the increase in the nondissociative double ionization observed in the TOF spectra for this trial, shown in the inset of Fig. 6(a). The multiple pulse structure shown in Fig. 12 is one of the common features of the pulses that maximize the $NO^{2+}/(N^+ + O^+)$ ratio. As shown in Fig. 17, the other $NO^{2+}/(N^+ + O^+)$ optimization trials at similar pulse energies had multiple pulses and a similar overall trend to the phase, although the details of both differ from each other and from Fig. 12. Still, the explanation developed for the most effective

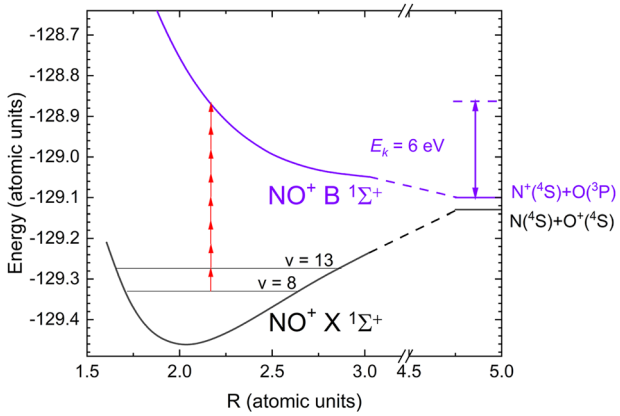

FIG. 16. Potential energy curves[125] for the NO^+ X $^1\Sigma^+$ (black line) and B $^1\Sigma^+$ (purple line) states. The v = 8 and v = 13 vibrational levels[126] of the X $^1\Sigma^+$ state are shown. The energies at the separate atom limits[126] are −128.79 a.u. for the NO^+ X $^1\Sigma^+$ state and −128.76 a.u. for the B $^1\Sigma^+$ state. The dissociative B $^1\Sigma^+$ state can be reached via eight 790 nm photons from the v = 8 state or seven photons from the v = 13 state of X $^1\Sigma^+$, both resulting in an E_k of 6 eV.

25 September 2023 21:20:00

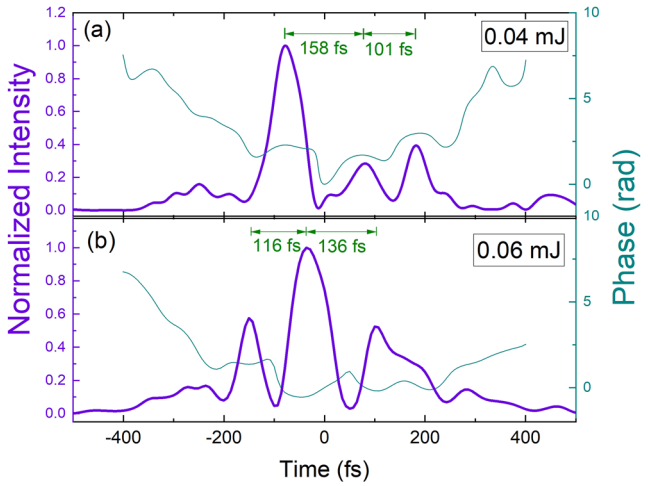

FIG. 17. The temporal intensity (thick purple) and phase (thin cyan) of the additional laser pulses that optimized $NO^{2+}/(N^+ + O^+)$ at pulse energies below 0.5 mJ. The temporal separation between the peaks of the different pulses is indicated in the figure. (a) The pulse that yielded $NO^{2+}/(N^+ + O^+) = 2.8 \pm 0.9$ at 0.04 mJ. (b) The pulse that resulted in $NO^{2+}/(N^+ + O^+) = 6.0 \pm 0.9$ at 0.06 mJ.

0.06 mJ pulse can reasonably be applied to the other optimized 0.06 mJ and 0.04 mJ pulses that are reported in Table I.

The efforts to use closed-loop coincidence feedback to both maximize and minimize the $NO^{2+}/(N^+ + O^+)$ ratio at intensities around 10^{14} W/cm^2 were successful, with all trials resulting in some enhancement or suppression of the ratio with the best exceeding a factor of 10. The VMI-based analysis yields additional information. First, the difference in the uncorrelated VMI measurements of the N^+ and O^+ fragments indicate that simply trying to use one of these fragments as a proxy for the $N^+ + O^+$ coincidence yield in the optimization feedback would not lead to the desired outcome, since there are clearly other channels, such as $N^+ + O$, present in the VMI data. This is true even in the same range of E_k where the $N^+ + O^+$ coincidences appear, so separation based on fragment energy would be difficult. The angular information derived from the VMI data assists in separating the various dissociation channels. Second, most of the control seems to be associated with an increase or decrease in the NO^{2+} yield, rather than significant changes in the number of $N^+ + O^+$ dissociative double-ionization events. From an analysis perspective, this is unfortunate, since VMI measurements on the nondissociative NO^{2+} just reveal a thermal distribution of ions. Still, the fragment VMI information, along with the CTOF-based $P(E_k)$ distributions, provides enough clues about the fragment behavior to allow us to indirectly surmise some plausible routes to the observed control. This analysis is helped by the nature of the pulse shapes, which are not extremely complex.

IV. SUMMARY AND OUTLOOK

Adaptive strong field control that uses coincidence-time-of-flight feedback has been successfully employed to control the ratio of nondissociative to dissociative double ionization $NO^{2+}/(N^+ + O^+)$ of NO molecules. The use of the CTOF feedback allowed the separation of the $N^+ + O^+$ ion pairs from the $N^+ + O$ or $N + O^+$ dissociative single ionization products. The $NO^{2+}/(N^+ + O^+)$ ratio was increased or decreased by about an order of magnitude at pulse energies between 0.04 and 0.06 mJ or around 10^{14} W/cm^2 for FTL pulses at our focusing conditions. Without the use of the CTOF feedback, it is unlikely that the optimization would have been possible due to the large magnitude of the dissociative single ionization channels and the range of intensities present in the laser focal volume.

The work by Rabitz and co-workers demonstrating the robustness of feedback-based optimization,[127–130] even in the face of experimental constraints, coupled with the experimental efforts that demonstrate how laser-induced Stark shifts can activate many unimolecular reaction pathways,[21,74–78] has led to an understanding that strong-field closed-loop control results cannot easily be "reverse-engineered" to gain knowledge of the control mechanism.[27,40] In this article, we show that when the laser intensity is not too high and the feedback is well-defined, CTOF and VMI analysis of the resulting photofragments identifies a plausible control mechanism that links the optimized pulse to the measured ion characteristics. More detailed theoretical efforts are required to confirm the mechanistic analysis presented here.

At higher energy (~0.5 mJ), the pulse complexity increases significantly, and determining the underlying molecular dynamics clearly becomes more difficult, although the control is at least as successful as at lower intensities.

In both intensity regimes, the role of focal volume averaging is limited by the CTOF technique, since the $N^+ + O^+$ coincidences are required to originate from the same charge state as the nondissociative NO^{2+} ions. The focal volume effect is not completely eliminated, however, since the dissociative and nondissociative NO^{2+} states have different energies, resulting in some ambiguities in the interpretation. That said, this work does not employ the sort of highly sophisticated, correlated, multihit electron-ion momentum imaging methods such as COLTRIMS/reaction microscopes[131] or advanced VMI methods.[132–135] Those techniques could potentially provide more differential information that might illuminate important dynamics and further restrict uncertainty due to focal volume averaging. This would be particularity interesting if highly differential experimental signals could be incorporated into the closed-loop control as feedback.

ACKNOWLEDGMENTS

We thank Bishwanath Gaire for his help with data collection and the group of Professor Zenghu Chang for assistance with the laser. Augustana University personnel and equipment were supported by the National Science Foundation Grant Nos. PHY-0969687 and PHY-1723002. J.R. Macdonald Laboratory personnel and equipment were supported by the Chemical Sciences, Geosciences, and Biosciences Division, Office of Basic Energy Science, Office of Science, U.S. Department of Energy under Award No. DE-FG02-86ER13491.

REFERENCES

[1] R. S. Judson and H. Rabitz, Phys. Rev. Lett. **68**, 1500 (1992).
[2] A. Assion, T. Baumert, M. Bergt, T. Brixner, B. Kiefer, V. Seyfried, M. Strehle, and G. Gerber, Science **282**, 919 (1998).

25 September 2023 21:20:00

[3]R. J. Levis, G. M. Menkir, and H. Rabitz, Science **292**, 709 (2001).
[4]H. Rabitz, Science **288**, 824 (2000).
[5]S. A. Rice and S. P. Shah, Phys. Chem. Chem. Phys. **4**, 1683 (2002).
[6]M. Shapiro and P. Brumer, Rep. Prog. Phys. **66**, 859 (2003).
[7]C. Brif, R. Chakrabarti, and H. Rabitz, New J. Phys. **12**, 075008 (2010).
[8]B. J. Pearson, J. L. White, T. C. Weinacht, and P. H. Bucksbaum, Phys. Rev. A **63**, 063412 (2001).
[9]J. L. Herek, W. Wohlleben, R. J. Cogdell, D. Zeidler, and M. Motzkus, Nature **417**, 533 (2002).
[10]T. Brixner, G. Krampert, T. Pfeifer, R. Selle, G. Gerber, M. Wollenhaupt, O. Graefe, C. Horn, D. Liese, and T. Baumert, Phys. Rev. Lett. **92**, 208301 (2004).
[11]G.-Y. Chen, Z. W. Wang, and W. T. Hill, Phys. Rev. A **79**, 011401 (2009).
[12]M. Kotur, T. Weinacht, B. J. Pearson, and S. Matsika, J. Chem. Phys. **130**, 134311 (2009).
[13]D. G. Kuroda, C. P. Singh, Z. Peng, and V. D. Kleiman, Science **326**, 263 (2009).
[14]M. Roth, L. Guyon, J. Roslund, V. Boutou, F. Courvoisier, J.-P. Wolf, and H. Rabitz, Phys. Rev. Lett. **102**, 253001 (2009).
[15]J. Plenge, A. Wirsing, I. Wagner-Drebenstedt, I. Halfpap, B. Kieling, B. Wassermann, and E. Ruhl, Phys. Chem. Chem. Phys. **13**, 8705 (2011).
[16]S. Singha, Z. Hu, and R. J. Gordon, J. Phys. Chem. A **115**, 6093 (2011).
[17]P. Nuernberger, D. Wolpert, H. Weiss, and G. Gerber, Phys. Chem. Chem. Phys. **14**, 1185 (2012).
[18]S. Rosi, A. Bernard, N. Fabbri, L. Fallani, C. Fort, M. Inguscio, T. Calarco, and S. Montangero, Phys. Rev. A **88**, 021601 (2013).
[19]I. R. Solá, J. González-Vázquez, R. de Nalda, and L. Bañares, Phys. Chem. Chem. Phys. **17**, 13183 (2015).
[20]M. Bergt, T. Brixner, B. Kiefer, M. Strehle, and G. Gerber, J. Phys. Chem. A **103**, 10381 (1999).
[21]R. J. Levis and H. A. Rabitz, J. Phys. Chem. A **106**, 6427 (2002).
[22]A. Bartelt, S. Minemoto, C. Lupulescu, Š. Vajda, and L. Wöste, Eur. Phys. J. D **16**, 127 (2001).
[23]M. Bergt, T. Brixner, C. Dietl, B. Kiefer, and G. Gerber, J. Organomet. Chem. **661**, 199 (2002).
[24]N. Damrauer, C. Dietl, G. Krampert, S.-H. Lee, K.-H. Jung, and G. Gerber, Eur. Phys. J. D **20**, 71 (2002).
[25]A. Lindinger, C. Lupulescu, M. Plewicki, F. Vetter, A. Merli, S. M. Weber, and L. Wöste, Phys. Rev. Lett. **93**, 033001 (2004).
[26]C. Trallero-Herrero, D. Cardoza, T. C. Weinacht, and J. L. Cohen, Phys. Rev. A **71**, 013423 (2005).
[27]E. Wells, K. J. Betsch, C. W. S. Conover, M. J. DeWitt, D. Pinkham, and R. R. Jones, Phys. Rev. A **72**, 063406 (2005).
[28]T. Laarmann, I. Shchatsinin, A. Stalmashonak, M. Boyle, N. Zhavoronkov, J. Handt, R. Schmidt, C. P. Schulz, and I. V. Hertel, Phys. Rev. Lett. **98**, 058302 (2007).
[29]T. Laarmann, I. Shchatsinin, P. Singh, N. Zhavoronkov, M. Gerhards, C. P. Schulz, and I. V. Hertel, J. Chem. Phys. **127**, 201101 (2007).
[30]B. J. Pearson, S. R. Nichols, and T. Weinacht, J. Chem. Phys. **127**, 131101 (2007).
[31]L. Palliyaguru, J. Sloss, H. Rabitz, and R. J. Levis, J. Mod. Opt. **55**, 177 (2008).
[32]J. González-Vázquez, L. González, S. R. Nichols, T. C. Weinacht, and T. Rozgonyi, Phys. Chem. Chem. Phys. **12**, 14203 (2010).
[33]Z. Hu, S. Singha, Y. Zhao, G. E. Barry, T. Seideman, and R. J. Gordon, J. Phys. Chem. Lett. **3**, 2744 (2012).
[34]T. Baumert, M. Grosser, R. Thalweiser, and G. Gerber, Phys. Rev. Lett. **67**, 3753 (1991).
[35]C. Daniel, J. Full, L. González, C. Lupulescu, J. Manz, A. Merli, S. Vajda, and L. Wöste, Science **299**, 536 (2003).
[36]D. Cardoza, C. Trallero-Herrero, F. Langhojer, H. Rabitz, and T. Weinacht, J. Chem. Phys. **122**, 124306 (2005).
[37]F. Langhojer, D. Cardoza, M. Baertschy, and T. Weinacht, J. Chem. Phys. **122**, 014102 (2005).
[38]D. Cardoza, B. J. Pearson, M. Baertschy, and T. Weinacht, J. Photochem. Photobiol., A **180**, 277 (2006).
[39]G. Vogt, P. Nuernberger, R. Selle, F. Dimler, T. Brixner, and G. Gerber, Phys. Rev. A **74**, 033413 (2006).
[40]J. L. White, E. C. Carroll, K. G. Spears, and R. J. Sension, Isr. J. Chem. **52**, 397 (2012).
[41]D. Geißler, P. Marquetand, J. González-Vázquez, L. González, T. Rozgonyi, and T. Weinacht, J. Phys. Chem. A **116**, 11434 (2012).
[42]R. R. de Castro, R. Cabrera, D. I. Bondar, and H. Rabitz, New J. Phys. **15**, 025032 (2013).
[43]E. Wells, C. Rallis, M. Zohrabi, R. Siemering, B. Jochim, P. Andrews, U. Ablikim, B. Gaire, S. De, K. Carnes, B. Bergues, R. de Vivie-Riedle, M. Kling, and I. Ben-Itzhak, Nat. Commun. **4**, 2895 (2013).
[44]X. Xing, R. R. de Castro, and H. Rabitz, New J. Phys. **16**, 125004 (2014).
[45]D. Geißler and T. Weinacht, Phys. Rev. A **89**, 013408 (2014).
[46]P. Sándor, A. Zhao, T. Rozgonyi, and T. Weinacht, J. Phys. B: At., Mol. Opt. Phys. **47**, 124021 (2014).
[47]X. Xing, R. R. de Castro, and H. Rabitz, J. Phys. Chem. A **121**, 8632 (2017).
[48]A. M. Weiner, Rev. Sci. Instrum. **71**, 1929 (2000).
[49]F. Verluise, V. Laude, Z. Cheng, C. Spielmann, and P. Tournois, Opt. Lett. **25**, 575 (2000).
[50]A. Monmayrant, S. Weber, and B. Chatel, J. Phys. B: At., Mol. Opt. Phys. **43**, 103001 (2010).
[51]E. Wells, J. McKenna, A. M. Sayler, B. Jochim, N. Gregerson, R. Averin, M. Zohrabi, K. D. Carnes, and I. Ben-Itzhak, J. Phys. B: At., Mol. Opt. Phys. **43**, 015101 (2010).
[52]R. Baková, J. Fišer, T. Šedivcová Uhlíková, and V. Špirko, J. Chem. Phys. **128**, 144301 (2008).
[53]B. Jochim, M. Zohrabi, B. Gaire, F. Anis, T. Uhlíková, K. D. Carnes, E. Wells, B. D. Esry, and I. Ben-Itzhak, "Direct evidence of the dominant role of multiphoton permanent-dipole transitions in strong-field dissociation of NO^{2+}," Phys. Rev. Lett. (submitted).
[54]D. W. Chandler and P. L. Houston, J. Chem. Phys. **87**, 1445 (1987).
[55]A. T. J. B. Eppink and D. H. Parker, Rev. Sci. Instrum. **68**, 3477 (1997).
[56]D. H. Parker and A. T. J. B. Eppink, J. Chem. Phys. **107**, 2357 (1997).
[57]*Imaging in Molecular Dynamics: Technology and Applications*, edited by B. J. Whitaker (Cambridge University Press, Cambridge, UK, 2003).
[58]C. E. Rallis, T. G. Burwitz, P. R. Andrews, M. Zohrabi, R. Averin, S. De, B. Bergues, B. Jochim, A. V. Voznyuk, N. Gregerson, B. Gaire, I. Znakovskaya, J. McKenna, K. D. Carnes, M. F. Kling, I. Ben-Itzhak, and E. Wells, Rev. Sci. Instrum. **85**, 113105 (2014).
[59]G. Floquet, Ann. Sci. Ec. Norm. Super. **12**, 47 (1883).
[60]A. Hishikawa, S. Liu, A. Iwasaki, and K. Yamanouchi, Chem. Phys. **114**, 9856 (2001).
[61]A. M. Sayler, P. Q. Wang, K. D. Carnes, B. D. Esry, and I. Ben-Itzhak, Phys. Rev. A **75**, 063420 (2007).
[62]B. Jochim, R. Averin, N. Gregerson, J. McKenna, S. De, D. Ray, M. Zohrabi, B. Bergues, K. D. Carnes, M. F. Kling, I. Ben-Itzhak, and E. Wells, Phys. Rev. A **83**, 043417 (2011).
[63]R. Trebino, *Frequency-Resolved Optical Gating* (Kluwer Academic Publishers, 2000).
[64]N. G. Kling, D. Paul, A. Gura, G. Laurent, S. De, H. Li, Z. Wang, B. Ahn, C. H. Kim, T. K. Kim, I. Litvinyuk, C. L. Cocke, I. Ben-Itzhak, D. Kim, and M. F. Kling, J. Instrum. **9**, P05005 (2014).
[65]W. C. Wiley and I. H. McLaren, Rev. Sci. Instrum. **26**, 1150 (1955).
[66]J. L. Wiza, Nucl. Instrum. Methods **162**, 587 (1979).
[67]E. Wells, M. Todt, B. Jochim, N. Gregerson, R. Averin, N. G. Wells, N. L. Smolnisky, N. Jastram, J. McKenna, A. M. Sayler, N. G. Johnson, M. Zohrabi, B. Gaire, K. D. Carnes, and I. Ben-Itzhak, Phys. Rev. A **80**, 063402 (2009).
[68]I. Ben-Itzhak, S. Ginther, and K. Carnes, Nucl. Instrum. Methods Phys. Res. B **66**, 401 (1992).
[69]I. Ben-Itzhak, S. G. Ginther, V. Krishnamurthi, and K. D. Carnes, Phys. Rev. A **51**, 391 (1995).
[70]M. J. J. Vrakking, Rev. Sci. Instrum. **72**, 4084 (2001).
[71]G. A. Garcia, L. Nahon, and I. Powis, Rev. Sci. Instrum. **75**, 4989 (2004).

25 September 2023 21:20:00

[72]G. M. Roberts, J. L. Nixon, J. Lecointre, E. Wrede, and J. R. R. Verlet, Rev. Sci. Instrum. **80**, 053104 (2009).
[73]C. Guo, Phys. Rev. A **71**, 021405 (2005).
[74]T. Bayer, M. Wollenhaupt, and T. Baumert, J. Phys. B: At., Mol. Opt. Phys. **41**, 074007 (2008).
[75]M. Krug, T. Bayer, M. Wollenhaupt, C. Sarpe-Tudoran, T. Baumert, S. S. Ivanov, and N. V. Vitanov, New J. Phys. **11**, 105051 (2009).
[76]J. G. Underwood, M. Spanner, M. Y. Ivanov, J. Mottershead, B. J. Sussman, and A. Stolow, Phys. Rev. Lett. **90**, 223001 (2003).
[77]B. J. Sussman, D. Townsend, M. Y. Ivanov, and A. Stolow, Science **314**, 278 (2006).
[78]C. Trallero-Herrero and T. C. Weinacht, Phys. Rev. A **75**, 063401 (2007).
[79]J. L. White, B. J. Pearson, and P. H. Bucksbaum, J. Phys. B: At., Mol. Opt. Phys. **37**, L399 (2004).
[80]M. A. Montgomery, R. R. Meglen, and N. H. Damrauer, J. Phys. Chem. A **110**, 6391 (2006).
[81]R. N. Zare, Mol. Photochem. **4**, 1 (1972).
[82]F. Légaré, I. V. Litvinyuk, P. W. Dooley, F. Quéré, A. D. Bandrauk, D. M. Villeneuve, and P. B. Corkum, Phys. Rev. Lett. **91**, 093002 (2003).
[83]A. S. Alnaser, X. M. Tong, T. Osipov, S. Voss, C. M. Maharjan, P. Ranitovic, B. Ulrich, B. Shan, Z. Chang, C. D. Lin, and C. L. Cocke, Phys. Rev. Lett. **93**, 183202 (2004).
[84]P. B. Corkum, Phys. Rev. Lett. **71**, 1994 (1993).
[85]M. Lewenstein, P. Balcou, M. Y. Ivanov, A. L'Huillier, and P. B. Corkum, Phys. Rev. A **49**, 2117 (1994).
[86]H. Niikura, F. Légaré, R. Hasbani, A. D. Bandrauk, M. Y. Ivanov, D. M. Villeneuve, and P. B. Corkum, Nature **417**, 917 (2002).
[87]A. S. Alnaser, T. Osipov, E. P. Benis, A. Wech, B. Shan, C. L. Cocke, X. M. Tong, and C. D. Lin, Phys. Rev. Lett. **91**, 163002 (2003).
[88]I. Znakovskaya, P. von den Hoff, S. Zherebtsov, A. Wirth, O. Herrwerth, M. J. J. Vrakking, R. de Vivie-Riedle, and M. F. Kling, Phys. Rev. Lett. **103**, 103002 (2009).
[89]K. Codling, L. J. Frasinski, and P. A. Hatherly, J. Phys. B: At., Mol. Opt. Phys. **21**, L433 (1988).
[90]K. Codling and L. J. Frasinski, Contemp. Phys. **35**, 243 (1994).
[91]S. Chelkowski and A. D. Bandrauk, J. Phys. B: At., Mol. Opt. Phys. **28**, L723 (1995).
[92]H. Stapelfeldt, E. Constant, and P. B. Corkum, Phys. Rev. Lett. **74**, 3780 (1995).
[93]S. Chelkowski, A. Conjusteau, T. Zuo, and A. D. Bandrauk, Phys. Rev. A **54**, 3235 (1996).
[94]A. D. Bandrauk and H. Z. Lu, Phys. Rev. A **62**, 053406 (2000).
[95]H. Ren, R. Ma, J. Chen, X. Li, H. Yang, and Q. Gong, J. Phys. B: At., Mol. Opt. Phys. **36**, 2179 (2003).
[96]Q. Liang, C. Wu, Z. Wu, M. Liu, Y. Deng, and Q. Gong, Phys. Rev. A **79**, 045401 (2009).
[97]K. Codling, L. J. Frasinski, and P. A. Hatherly, J. Phys. B: At., Mol. Opt. Phys. **22**, L321 (1989).
[98]T. Zuo and A. D. Bandrauk, Phys. Rev. A **52**, R2511 (1995).
[99]T. Seideman, M. Y. Ivanov, and P. B. Corkum, Phys. Rev. Lett. **75**, 2819 (1995).
[100]S. Chelkowski, T. Zuo, O. Atabek, and A. D. Bandrauk, Phys. Rev. A **52**, 2977 (1995).
[101]T. Zuo and A. D. Bandrauk, Phys. Rev. A **54**, 3254 (1996).
[102]J. H. Posthumus, A. J. Giles, M. R. Thompson, W. Shaikh, A. J. Langley, L. J. Frasinski, and K. Codling, J. Phys. B: At., Mol. Opt. Phys. **29**, L525 (1996).
[103]C. R. Scheper, W. J. Buma, C. A. de Lange, and W. J. van der Zande, J. Chem. Phys. **109**, 8319 (1998).
[104]A. Saenz, Phys. Rev. A **61**, 051402 (2000).
[105]J. H. Posthumus, B. Fabre, C. Cornaggia, N. de Ruette, and X. Urbain, Phys. Rev. Lett. **101**, 233004 (2008).
[106]J. McKenna, M. Suresh, B. Srigengan, I. D. Williams, W. A. Bryan, E. M. L. English, S. L. Stebbings, W. R. Newell, I. C. E. Turcu, J. M. Smith, E. J. Divall, C. J. Hooker, A. J. Langley, and J. L. Collier, Phys. Rev. A **73**, 043401 (2006).
[107]G. L. Kamta and A. D. Bandrauk, Phys. Rev. Lett. **94**, 203003 (2005).
[108]G. L. Kamta and A. D. Bandrauk, Phys. Rev. A **76**, 053409 (2007).
[109]A. Bandrauk and F. Légaré, in *Progress in Ultrafast Intense Laser Science VIII*, edited by K. Yamanouchi, M. Nisoli, and W. T. Hill III (Springer-Verlag GmbH, 2012).
[110]B. Gaire, J. McKenna, N. G. Johnson, A. M. Sayler, E. Parke, K. D. Carnes, and I. Ben-Itzhak, Phys. Rev. A **79**, 063414 (2009).
[111]A. Talebpour, S. Larochelle, and S. L. Chin, J. Phys. B: At., Mol. Opt. Phys. **30**, 1927 (1997).
[112]C. Guo and K. Wright, Phys. Rev. A **71**, 021404 (2005).
[113]C. Guo and K. Wright, Phys. Rev. A **74**, 019904 (2006).
[114]C. Guo, J. Phys. B: At., Mol. Opt. Phys. **38**, L323 (2005).
[115]J. Wu, H. Zeng, and C. Guo, Phys. Rev. A **74**, 031404 (2006).
[116]J. Wu, H. Zeng, and C. Guo, J. Phys. B: At., Mol. Opt. Phys. **39**, 3849 (2006).
[117]J. H. Posthumus, J. Plumridge, M. K. Thomas, K. Codling, L. J. Frasinski, A. J. Langley, and P. F. Taday, J. Phys. B: At., Mol. Opt. Phys. **31**, L553 (1998).
[118]F. Rosca-Pruna, E. Springate, H. L. Offerhaus, M. Krishnamurthy, N. Farid, C. Nicole, and M. J. J. Vrakking, J. Phys. B: At., Mol. Opt. Phys. **34**, 4919 (2001).
[119]J. H. Posthumus, Rep. Prog. Phys. **67**, 623 (2004).
[120]K. Miyazaki, T. Shimizu, and D. Normand, J. Phys. B: At., Mol. Opt. Phys. **37**, 753 (2004).
[121]X. M. Tong, Z. X. Zhao, A. S. Alnaser, S. Voss, C. L. Cocke, and C. D. Lin, J. Phys. B: At., Mol. Opt. Phys. **38**, 333 (2005).
[122]F. Anis, T. Cackowski, and B. D. Esry, J. Phys. B: At., Mol. Opt. Phys. **42**, 091001 (2009).
[123]X. M. Tong, Z. X. Zhao, and C. D. Lin, Phys. Rev. A **66**, 033402 (2002).
[124]S. Voss, A. S. Alnaser, X.-M. Tong, C. Maharjan, P. Ranitovic, B. Ulrich, B. Shan, Z. Chang, C. D. Lin, and C. L. Cocke, J. Phys. B: At., Mol. Opt. Phys. **37**, 4239 (2004).
[125]I. Rabadán and J. Tennyson, J. Phys. B: At., Mol. Opt. Phys. **30**, 1975 (1997).
[126]D. L. Albritton, A. L. Schmeltekopf, and R. N. Zare, J. Chem. Phys. **71**, 3271 (1979).
[127]G. J. Tóth, A. Lőrincz, and H. Rabitz, J. Chem. Phys. **101**, 3715 (1994).
[128]H. A. Rabitz, Science **303**, 1998 (2004).
[129]K. W. Moore, A. Pechen, X.-J. Feng, J. Dominy, V. J. Beltrani, and H. Rabitz, Phys. Chem. Chem. Phys. **13**, 10048 (2011).
[130]C.-C. Shu, T.-S. Ho, X. Xing, and H. Rabitz, Phys. Rev. A **93**, 033417 (2016).
[131]J. Ullrich, R. Moshammer, A. Dorn, R. Dörner, L. P. H. Schmidt, and H. Schmidt-Böcking, Rep. Prog. Phys. **66**, 1463 (2003).
[132]A. T. Clark, J. P. Crooks, I. Sedgwick, R. Turchetta, J. W. L. Lee, J. J. John, E. S. Wilman, L. Hill, E. Halford, C. S. Slater, B. Winter, W. H. Yuen, S. H. Gardiner, M. L. Lipciuc, M. Brouard, A. Nomerotski, and C. Vallance, J. Phys. Chem. A **116**, 10897 (2012).
[133]A. Zhao, M. van Beuzekom, B. Bouwens, D. Byelov, I. Chakaberia, C. Cheng, E. Maddox, A. Nomerotski, P. Svihra, J. Visser, V. Vrba, and T. Weinacht, Rev. Sci. Instrum. **88**, 113104 (2017).
[134]A. Zhao, P. Sándor, and T. Weinacht, J. Chem. Phys. **147**, 013922 (2017).
[135]J. Long, F. J. Furch, J. Durá, A. S. Tremsin, J. Vallerga, C. P. Schulz, A. Rouzée, and M. J. J. Vrakking, J. Chem. Phys. **147**, 013919 (2017).

25 September 2023 21:20:00